State conditional optogenetic entrainment of the septo-hippocampal circuit reveals the importance of endogenous theta oscillations as a unit of spatial metric

Philippe R. Mouchati[1], Gregory L. Holmes[1], Jeremy M. Barry[1]

Running Head: State conditional optogenetic entrainment of the septo-hippocampal circuit

Author Affiliations:

[1]Epilepsy Development and Cognition Group, Department of Neurological Sciences, University of Vermont, Larner College of Medicine, Burlington, Vermont

Corresponding Author:

Jeremy M. Barry, PhD
Department of Neurological Sciences
University of Vermont College of Medicine
89 Beaumont Avenue
Burlington, VT 05405
Phone: (802) 656-4588
Fax: (802) 656-5678

Key words: Oscillations, Cognition, Theta, Optogenetics, Spatial Accuracy, Circuit State

Acknowledgements: We are very appreciative of Colin Lever, Dr. Matt Wilson, Dr. Nathan Insel, Dr. Andre Fenton, and Dr. Allan Gulledge who shared their thoughts on analysis and the interpretation of our results. We thank Andrew Alvarenga (GMW) for assistance with the custom design and manufacture of optical and electrophysiological implants. We thank Bruno Rivard, Rhys Niedecker and Kate Van Pelt for assistance with components of Figure 1. We are grateful for COBRE support from Sheryl White who greatly assisted with immunohistochemistry. We thank Pierre Pascal Lenck-Santini, Sylvain Barriere and Sophie Sakkaki for assistance with Matlab code used for signal processing. We thank Mr. Daniel Mills for superb editing. We also acknowledge Neuralynx (Montana, USA) for dedicated technical support and Karl Deisseroth for supplying the adenovirus used in the study. This work would not have been possible without the advice of Dr. John Kubie for developing and implementing the spatial accuracy task. We declare no conflicts of interest.

Author Contributions: P.R.M and J.M.B collected data; J.M.B designed the experiments and analyzed the data. All authors wrote the paper.

Summary

Mechanisms by which pattern generators impose temporal organization on target nodes while reacting to changes in behavior and cognitive demand remain poorly understood. While perturbation through optogentic stimulation can reveal circuit mechanisms that create and locally integrate this temporal organization, it is unclear whether superseding endogenous signals with artificial oscillations would benefit or impede hippocampus-dependent cognition or how cognitive demand might affect septo-hippocampal entrainment. Optogenetically stimulating the MS of wild-type rats in 3 contexts showed that septal input supersedes endogenous hippocampal oscillations when animals are at rest and while performing a hippocampus-dependent spatial accuracy task. Stimulation during a hippocampus-independent task, however, resulted in endogenous compensatory oscillations. Although burst-timing organization of hippocampal cells mirrored task-conditional theta entrainment, place field properties were unaffected. Impairment with regard to spatial accuracy behavior in the hippocampus-dependent task underscores the role of theta oscillations in the computation of spatial metric.

Introduction

A fundamental feature of the brain is its dynamic organization in time. One of the central pursuits of neuroscience is to determine how central pattern generators govern the reciprocal temporal relationship between oscillations and synchronized cell assemblies, within and between neural circuits, is [1-3]. Specifically, the mechanism by which pattern generators in one node of a neural circuit entrain target nodes while dynamically responding to changes in behavior or cognitive demand remains one of the most important queries yet to be imposed upon the properties of emergent networks.

Theta oscillations are the largest amplitude local field potentials in the hippocampus. They are associated with exploratory behavior and are principally generated by cortical afferents to the distal apical dendrites of pyramidal cells [4-6]. The pace of the waxing and waning of rhythmic theta oscillations at 5 -12 Hz corresponds to membrane potential fluctuations that reflect the temporal synchronization of neural activity on an 83 – 200 ms timescale. The *in vivo* pacing of theta frequency [7, 8] has been proposed to be dictated by the theta pattern generator in the MS (Medial Septum) that generates rhythmic disinhibition at the synapses of hippocampal pyramidal neurons via long-range axons from the MS to hippocampal GABAergic neurons [9-13]. This septal feed-forward inhibition contributes to the coordination of state dependent network activity through terminal projections that target both specific areas and cell types in the hippocampus [14, 15], influencing the alternation of discharge probability in neurons across the septo-temporal axis [16-18] and the entorhinal-hippocampal loop [19].

Modeling and experimental work have suggested that theta phase relationships of both synaptic current and cellular action potentials are important for the encoding and retrieval of memories [20-22] and the self-motion based estimation of linear distance through the integration of speed, distance and time [23-26]. These critical and often interdependent cognitive processes [27] are both accomplished by the phasic routing of neural throughput within and between the hippocampus and neocortex. The temporal discoordination of action potentials relative to theta, due to pharmacological or gene manipulation or as a result of status epilepticus in early life, has been shown to correlate with impairment to memory [28, 29] and performance deficits in a complex spatial task [30].

Selective optogenetic artificial theta band stimulation of GABAergic [31] or glutamatergic [13, 32] components of the septal pacemaker in transgenic mice has been shown to supersede endogenous hippocampal theta frequency. Non-selective optogenetic stimulation of the MS has also been carried out in wild-type rats and has been shown to match hippocampal theta frequency in a 1:1 fashion [33, 34], with the caveat that stimulation during speeds greater than 5 cm/s bisects hippocampal theta frequency between the septal input frequency and an endogenous compensatory frequency [34]. Optogenetic stimulation studies therefore have the

potential to address several open questions regarding the mechanisms by which the septal pacemaker entrains or competes with hippocampal oscillations. It also has the potential to function as a neuroprosthetic for ameliorating cognitive disabilities caused by theta rhythmopathy in diseases such as temporal lobe epilepsy [35]. While correcting errant circuits for the benefit of cognitive dysfunction is the great promise of optogenetics, no studies have yet demonstrated that superseding endogenous signals with artificial oscillations would act to the benefit or detriment of hippocampus-dependent cognition. Moreover, how changes in cognitive demand might affect the efficacy of septo-hippocampal entrainment is still unknown. This gap in our understanding of the parameters by which systems level manipulation of neural circuits might attenuate temporally discordant networks precludes our ability to employ novel technologies aimed at treating associated cognitive deficits.

We therefore carried out two experiments that titrated behavior during non-selective optogenetic septal stimulation. We first stimulated during limited mobility, when there was less intrinsic hippocampal theta to compete with artificial theta input. We then stimulated during 2 versions of a spatial accuracy behavioral task, where the goal zone was cued or uncued. The cued version of the task is hippocampus-independent while the uncued version is hippocampus-dependent. The results of these experiments indicate that cognitive demands dictate circuit state, which dictates, in turn, the efficacy of septal entrainment of hippocampal theta. The results also support the notion that endogenous theta oscillations are necessary for self-localization metric.

Methods

Subject details

Seven male Sprague-Dawley rats (obtained from Charles River, Montreal), 3-8 months old were subjects in this study. Animals were housed individually and maintained on a 12 hour light/dark cycle and 85% of baseline body weight and given free access to water. All procedures were approved by the University of Vermont's Institutional Animal Care and Use Committee and conducted in accordance with guidelines from the National Institutes of Health.

Injection Surgery

At approximately 3 months old, 4 animals underwent the surgical procedure for the intracranial injection. Rats were anesthetized with a mixture of 5% inhaled isoflurane in oxygen and placed in a stereotaxic frame. All stereotaxic coordinates were relative to Bregma [36]. The skull was exposed and a burr hole was placed in the skull. A Hamilton injection syringe was then used to deliver 1 µl bolus injections of the AAV vector (AAV2-hSyn-hChR2(H134R)-EYFP; 5.7 x 10^{12} virus molecules/ml; UNC Vector Core, Chapel Hill, NC) at a rate of 0.1 µl/min into the vertical limb of the diagonal band of Broca in the MS (AP = 0.7 mm; ML= -1.4 mm) and angled 12° medially. The first injection of 0.15 µl was made at a depth of 7.1 mm from brain surface. The syringe was

retracted 3 times at 0.3mm steps with injections of 0.2 µl, 0.25 µl and 0.2 µl at each consecutive step. In the final step, the needle was raised 0.2 mm to a final depth of 6.0 mm and an ultimate injection of 0.2 µl was made. The wound was sutured and the rats were returned to their home cages to recover.

Examples of immunohistochemistry of ChR2 transfection in the MS, including expression of ChR2 in cholinergic and GABAergic cells, can be seen in Fig. 1A. The transfected axonal projections of these septal cells to interneurons in layers of CA1 in hippocampus are also shown.

Optical fiber and hippocampal tetrode implants

Detailed descriptions of the optical fiber preparation can be found in a previous publication and are described in brief here [34]. We used a 200 µm multimode optic fiber (Thorlabs, CFLC230-10; Montreal, Canada) as part of our chronic septal implant. The optical fiber was then glued to a 230 µm ferrule (Thorlabs, CFLC230-10; TP01235931). The percentage transmittance of light through the fiber was tested using 100% blue light transmittance (Spectralynx LED source) and measured by a light meter with a photodiode sensor (Thorlabs; Model PM100D). For testing purposes a 50 µm patch cable was used and only fibers that allowed for at least 70% light transmittance at approximately 0.5 mm from the tip of the optical fiber. The MS implant included an optic fiber with an array of 8 recording electrodes glued to the surface that extended 0.25-0.5 mm from the end of the optic fiber. The custom hippocampal implant consisted of 8 separately drivable tetrodes (32 channel electrode array; 'BLAK drives'; Grasshopper Machine Works, New Hampshire, USA). Each tetrode was composed of 4 wound 25 µm diameter nichrome wires (California Fine Wire, CA, USA). Each electrode was connected to custom millimax pins (Neuralynx, Montana, USA).

Optical probe and electrode array chronic implantation surgery

Approximately 2 weeks post-injection, a second surgery was carried out in order to chronically implant the custom microdrives into the left hippocampus (+ 3.3 mm ML; - 4.5 AP; - 2.0 DV). The optical/recording ensemble was lowered into the MS along the same path previously taken by the Hamilton injection syringe, with the end of the optical fiber lowered to a final depth of ~ 6.5 mm below brain surface. An illustration of the experimental approach using hippocampal septal and hippocampal implants can be seen in Fig. 1B.

Four skull screws (FHC Inc.) were inserted, two were anterior to bregma while the 2 remaining screws were placed over the left and right of the cerebellum. Grounding was achieved via connection to the right cerebellar screw while a reference wire was placed through a small burr hole at brain surface over the cerebellum. Both implants were fixed to the skull via the skull screws and Grip Cement (Dentsply Inc.). The wound was sutured and topical antibiotic applied. The interval between surgery and the beginning of electrophysiological recording was 1 week.

Stimulation and recording protocols

A 200 µm multimode optic fiber (Thor Laboratories, Budapest, Hungary) was used to connect the implanted optic fiber's 1.25 ceramic ferrule to Spectralynx, a computer controlled optical LED system (Neuralynx, Montana, USA). The pulse program (Neuralynx, Montana) was used to stimulate the rats with experimental B (wavelength 470-490nm) and control Y (wavelength 590nm). Maximum light intensity was set to 100% (1.8-2.2mW). Light transmittance to the MS via the chronically implanted optical fiber ranged from 70-85%, at the fiber tip. Sine wave stimulatory patterns were generated using the Pulse program (Neuralynx, Montana). Stimulation frequencies at 6 Hz (on/off 83.3 msec) and 10 Hz (on/off 50.6 msec) were generated in a sine wave pattern by creating an ascending and descending light intensity gradient during the "on" portion of the stimulation with a mean light intensity of 52%. The light stimulation was divided into 23 epochs corresponding to 0-255 bits where each increment was a percentage of peak amplitude at 255 bits (i.e., ranging from 1.6 to 100%). The frequency of the generated sine waves had a light duration of 3.6 msec and 2.2 msec for 6 and 10 Hz stimulation patterns respectively.

We chose 6 Hz as the primary stimulation frequency as much of the earlier septal stimulation literature noted that hippocampal cells were driven best at frequencies within the 6-8 Hz range. We also wished to move theta frequency enough from the mean frequency during movement, typically 7.5 Hz, in a manner that would be statistically and functionally distinguishable from baseline endogenous theta oscillations. This frequency would also be more likely to elicit a behavioral effect, as per the experimental hypothesis. We also stimulated at 10 Hz so we could compare entrainment efficacy between higher and lower ends of the theta band in relation to task performance.

Stimulations took place in 3 contexts in order to titrate the rat's behavior so as to control for the influence of movement and cognition on the background of the septo-hippocampal circuit and to understand how these variables affected the efficacy of hippocampal entrainment by optogenetic stimulation of the MS.

Flowerpot: Recording sessions were made while rats rested in a 40 cm high ceramic flowerpot that was 27 cm wide at the base and lined with home cage bedding. The size of the ceramic pot limited the rat's movements to rearing and minor head movements and therefore limited theta oscillations associated with active exploration. The experiment began without stimulation for 2 min, followed by 6 min of 6 Hz yellow spectrum stimulation (Y), then 6 min of 6 Hz B spectrum stimulation (B) and ending with an additional 2 min without stimulation.

The flowerpot also served as the location for screening session following the lowering of microdrives. Electrodes were advanced until they contacted the pyramidal cell layer in the CA1 field of the dorsal hippocampus, as characterized by the observation of clustered units as well as

140-200 Hz ripple activity in the local field potentials. Experimental sessions were carried out in the spatial accuracy task when > 20 hippocampal cells were isolated.

Cued and uncued spatial accuracy task: During exploration of a 75 cm diameter grey arena, a food-restricted rat learns that entry into an invisible circular target zone triggers an overhead pellet feeder [37]. The rat's location in the arena was sampled at 30 Hz (Tracker, Bio-signal Group Corp, Brooklyn, USA) using a firewire digital camera that detected a dark area behind the rat's head that was made with non-toxic, black permanent marker. When the rat's position was detected in the goal zone, the computer sent a +5V TTL pulse via the PCI board to a custom pellet feeder and triggered the release of a food pellet. For initial training, the center of the target area was marked with a 20 mm diameter bottle cap. Thirty-min training sessions are carried out each day with a refractory reward period of 5 sec and gradual progression of target zone area from 16 to 8 cm in diameter and target dwell time from 0.5 to 1.2 s. Next, uncued sessions were alternated with cued sessions. Importantly, between cued and uncued sessions rats were placed in the flowerpot alongside the arena for approximately 5 min. During this time the floor panel was cleaned with soap and water and rotated, while keeping a white cue card that covered approximately 90° fixed with relation to the room frame. In both task versions, criterion was set to 40 rewards in 3 consecutive sessions. Similar to cued and uncued versions of the Morris water maze, cued spatial accuracy is considered to be hippocampus-independent while the uncued version is considered to be hippocampus-dependent [38].

After meeting criterion with goal diameter at 8 cm, the animals underwent the septal injection of the AAV2 virus expressing ChR2 and given a week to recover. The rats were then implanted with the optical probe and electrode array described in Fig. 1. Screening sessions began after an additional week of recovery. Rats underwent additional training to ensure that they were still performing at criterion and that the surgical procedures and being tethered to the electrophysiology cables and the optical patch cable did not interfere with behavior. Each rat experienced a series of 3-4 experiments that began with the cued and uncued versions of the task with continuous open-loop 6 Hz Y for 30 min each. The rats were then disconnected for approximately 1 hour and returned to their home cages. As in the control stimulation sessions, B stimulation was open loop at 6 Hz for 30 min each and the order was randomized for each context. Only 1 of 2 MS stimulation frequencies was used each day (6 or 10 Hz).

Our design of the spatial accuracy task allowed for several behavioral metrics of the animal's ability to self-localize relative to the goal zone. These measures included the number of triggered rewards and the number of goal zone entrances. We also utilized the complementary measures of dwell-time and speed in order to both graphically depict the animal's choice behavior and calculate search parameters independent of reward. In particular, we used speed measures relative to the target zone center in order to calculate search accuracy. This was calculated using

convolution windows (Matlab, Mathworks Inc.) to find continuous bouts of slow movement (≤ 3 cm/s) between a lower bound of 1.2 s and an upper bound of 20 s within the target quadrant. The mean distance from each of these epochs from the target center was then calculated. The mean location of these epochs was then plotted as a center location in relation to the mean diameter of the scatter, or how far each epoch was from the target center. The corresponding circle was then used as a graphic depiction of the search accuracy in relation to the goal.

Foraging: Three additional animals were used as non-stimulated controls. These animals foraged for food pellets that fell at regular 30 sec intervals from the overhead feeder while evenly sampling the surface area of the recording chamber. Rats experienced 2 consecutive foraging sessions and were held in the flowerpot for approximately 5 min between sessions, in which time the arena floor was cleaned. In this context we wished to know how successive sessions in the recording environment would affect the properties of theta oscillations. A further question was how foraging for food pellets would relate to the cued version of the spatial accuracy task, with regard to the resultant theta phase population vectors, given that both tasks do not require cognitive demand. Results of a previous study predict that foraging does not tend to lead to tight temporal control of CA1 cell activity by local theta oscillations [30].

Position tracking

The rat's location in the arena was sampled using a digital camera that detected a light emitting diode (LED) placed near the back of the animal's head. This tracking information was filtered and recorded utilizing custom software (Neuralynx, Montana, USA) that allowed for the synchronization of the rat's position and speed with properties of the recorded cell and EEG signals. During recording sessions, the Bio-signal Tracker program was switched to light tracking mode in order to detect the LED and to trigger the release of food pellets.

Signal processing

Rats were tethered to a recording cable during recording sessions in all contexts. Signals were pre-amplified X 1 at the headstage and channeled through the tether cable to the signal amplifiers and computer interface. Sampling frequency (SF) of LFPs was at 30.3 KHz and filtered at 1-9000 Hz (Neuralynx, Montana), subsampled offline at 3000 Hz. LFP's were referenced against a 50 μm diameter stainless steel wire (California Fine Wire, CA, USA) placed at brain surface over the cerebellum. LFPs were processed offline using custom software that utilized the Matlab 'spectrogram' function (window = SF, overlap = SF/2) to calculate measures of signal amplitude and frequency in the theta band at 5-12 Hz via short-time Fourier transformation.

Frequency: Mean frequency in the theta band was calculated for the flowerpot recordings during each 6 min epoch of Y and B stimulation as well as in each Y and B condition during performance of the cued and uncued spatial accuracy task, independently of animal speed. Peak frequency

was determined at the frequency of the maximum amplitude of the speed filtered mean spectral signal during both slow movement speeds (≤ 2 cm/s) and fast movement speeds (between 5 and 50 cm/s).

Amplitude: Mean amplitude in the theta band was calculated for the flowerpot recordings during each 6 min epoch of Y and B stimulation as well as in each Y and B condition during performance of the cued and uncued spatial accuracy task, independently of animal speed. Amplitude was normalized by the sum of the . Peak amplitude was determined by the maximum value of the non-normalized speed sorted mean spectral signal during both slow movement speeds (≤ 2 cm/s) and fast movement speeds (between 5 and 50 cm/s).

Speed/Theta: As in previous work [34, 39], we analyzed the linear relationship between animal speed and theta band frequency during each version of the spatial accuracy task as well as during foraging sessions in non-stimulated control animals.

Unit isolation and classification: Single units were sampled at 30.3 KHz and filtered at 300-6000 Hz (Neuralynx, Montana). All tetrode signals were referenced against a tetrode wire near the corpus callosum. The activity of individual units was separated offline into different clusters based on their waveform properties. Waveform properties were defined in 3-dimensional feature space using custom spike-sorting software (Plexon, Dallas, TX). The primary quantitative measure of cluster quality provided by OFS (Offline Sorter) was J3, a non-parametric measure of the quality of sorting [40]. Finally, spikes that had a refractory period of less than 1 ms and units that were not determined to be pyramidal cells or interneurons [41, 42] were removed from analysis. Putative OLM and basket cell activity were distinguished via estimated recording depth, theta amplitude, phase preference[43] and phase offset between recording sites in order to distinguish between stratum Oriens and stratum Pyramidale. Pyramidal cells, interneurons and axonal activity were distinguished from each other via activity and waveform properties as described previously [41, 42, 44].

Temporal autocorrelation and corresponding periodicity: Spike times were binned at 10 ms intervals for each cell during flowerpot recordings and during spatial accuracy recordings in each stimulation and task condition. Autocorrelations between spike times [45] were computed from the resulting speed filtered vector (≥ 2 cm/s) via the Matlab cross-correlation function ('xcorr') that measures the similarity between the vector and the shifted (lagged) copies of the vector as a function of the lag. Autocorrelation histograms were plotted based on these autocorrelations that not only illustrated changes in the temporal organization of inter-spike intervals but any potential change in the number of events that might be caused by B stimulation. A variation of the cross-correlation function ('coeff') was used in order to generate correlations equal to 1 at lag times equal to 0. The resulting autocorrelogram was then used to calculate the modulation periodicity

between epochs of peak correlation as well as the magnitude of the modulation as determined by the depth between the peaks and troughs of the autocorrelogram (Supp. Fig.1). Modulation frequency was determined through the reciprocal of the periodicity.

Place cell firing fields: Several firing field properties were analyzed in order to determine the effect of task and stimulation condition on the spatial tuning of hippocampal cells as well as to verify whether or not each unit met place cell criteria [46]:

Firing rate - The number of action potentials fired by the cell in the firing field divided by dwell-time in the field. Only cells with an average in-field firing rate < 9 Hz were included in the data set. This threshold was set to avoid including putative interneurons. The mean overall firing rate was also determined by dividing the total number of action potentials by the length of the recording session.

Firing field coherence - Coherence was calculated as previously described [46] and estimates the regularity of the firing rate transition from pixel to pixel in relation to the spatial firing distribution. Cells with field coherence values > 0.2 were considered to be place cells.

Field size - The field size of firing fields ranged between a minimum of 9 contiguous pixels and a maximum of 700 pixels (approximately 60% of the arena surface).

Firing field stability - Positional firing stability was estimated from the similarity of the place cell's spatial firing pattern between each stimulation and task condition during spatial accuracy performance. Direct comparisons were made between Y and B stimulation sessions during the uncued task, Y and B stimulation sessions during the cued task and Y stimulation sessions during the cued and uncued task. Similarity is defined as the Fisher z-transform of the product-moment correlation between the firing rates in corresponding pixels for both intervals.

Phase preference: The tuning of each cell's action potentials to the theta band in the local field potential was analyzed via phase preference analysis as in previous studies [30]. Several criteria were imposed on the selection reference channel that served as the representative LFP signal for each tetrode. LFPs were only considered if they exhibited 140-200 Hz ripple activity, when the rat was at rest, and the wire had at least one cell. The selected LFP was filtered between 4-14 Hz using Chebyshev type 2 filters, then the phase was extracted using the Hilbert transform. All the spikes recorded from this tetrode and from neighboring tetrodes were assigned a phase value from the ongoing theta phase from the referenced LFP. The trough of the theta cycle was assigned to 0°/360° while the peak of the theta cycle was assigned to 180°. The mean preferred phase of firing was calculated for each cell by averaging the angle of each spike divided by the total spike count. Cells were considered to exhibit a significant phase preference when the p-value calculated with Rayleigh's test for non-uniformity of circular data [46] was determined at $p \leq$

0.01 Rayleigh's test for non-uniformity of circular data was calculated as [*Rbar* = *n*r*] [47] where n is the sum of the number of incidences in cases of binned angle data and r is the resultant vector length of the distribution. The angle (Dir) and length of the resultant vector (RBAR) for the individual cell and the population of cells for each rat were then calculated and plotted for each stimulation condition in both experiments. As a compliment to RBAR, we also measured population dispersion levels [$\delta = 1 - T_2 / (2 * RBAR^2)$] [47] and measured the variability of the population vector relative to theta cycle. If the population RBAR levels are low, dispersion levels should be high.

To test the changes in the circular distribution of preferred firing phase between stimulation conditions in experiment 1, we used the parametric Watson-Williams multi-sample test for equal means, used as a one-way analysis of variance for circular data [48]. This analysis was not performed if phase preference was determined to be non-significant in one of the recording contexts.

Statistical Analyses

As the behavioral, single unit and EEG datasets contain data from multiple sessions in a repeated measures design in single animals, the assumptions of independence of observations are invalid. The observations for each of these measures within single animals are likely to be correlated and these data can be represented as a cluster. In this case, the existence of a relationship between each measure of interest within an individual animal may then be assumed [49]. We therefore used GEE (SPSS; Armonk, NY), a class of regression marginal model, for exploring multivariable relationships between clustered signal property data or behavioral measures for individual animals sorted by stimulation/task condition. Unless otherwise indicated, analyses are by rat. The model was adjusted according to the distribution of each analyzed variable, i.e., gamma with log link models were used for non-normally distributed data while poisson loglinear distributions were used for count data.

Histological procedures

Rats received a lethal dose of isoflurane and were perfused intracardially with saline followed by 4% formaldehyde. The brains were extracted and stored in 4% formaldehyde and frozen coronal sections (30 μm) were cut and stained with cresyl violet. Electrode and probe positions in the MS and hippocampus were assessed in all rats, as was the extent of ChR2 transfection in the MS. Examples can be found in Supp. Fig. 2. Immunohistochemistry was carried out on representative sections from the MS and hippocampus using a cryostat. Septal sections were stained with anti-choline acetyltransferase (polyclonal rabbit anti-ChAT antibody, Synaptic Systems), anti-glutamate decarboxylase 2 (polyclonal guinea pig anti-GAD 2, Synaptic Systems), and anti-Vglut2 (polyclonal chicken, Synaptic Systems). All imaging was performed in SPOT 5.0

advanced imaging software (SPOT Imaging Solutions, Michigan, USA) using a Nikon DS-Fi1 color digital camera on a Nikon E400 microscope with FITC, TRITC, and DAPI filter set. Two 20x images were taken from septal sections of each animal stained for GABAergic, cholinergic and glutamatergic neurons. The image analysis software Fiji was used to quantify cell counts, utilizing the program's built-in grid macro and cell count plugins. Cells were considered co-localized when GAD/ChAT/VGLUT and GFP overlapped. Only cells with distinct nuclei as determined by the presence of DAPI were considered to be representative examples (See Fig.1A).

Results

We examined the role of the septo-hippocampal circuit state on optogenetic entrainment using two experiments. In experiment 1 (N= 3), 6 Hz Y and B MS stimulation was carried out while animals rested in a flowerpot. In this context, we hypothesized that there would be less competition between endogenous hippocampal theta and artificial theta oscillations without movement or cognitive demand. In experiment 2 (N= 3), animals performed a spatial accuracy task where the goal zone was either cued (C) or uncued (UC). In the cued context the task is hippocampus-independent while in the uncued context the task is hippocampus-dependent[38]. Each task was repeated to allow for comparison between continuous, open-loop 6 Hz Y and B MS stimulation during each session (Yellow Cued = YC, Yellow Uncued = YUC, Blue Cued = BC, Blue Uncued = BUC). We hypothesized that changes in cognitive demand between the cued and uncued tasks would affect the septo-hippocampal circuit in a manner that would influence the efficacy of hippocampal entrainment. In order to compare the different temporal phenomena in the hippocampus during movement but in the absence of cognitive demand, we also carried out electrophysiological recordings from an additional 3 animals while foraging for food pellets.

Experiment 1

MS optical stimulation entrains hippocampal theta band oscillations

As illustrated in Fig. 2A, 6 Hz B stimulation in the MS entrains oscillations in the MS and hippocampus. Example spectrograms for Y and B stimulation in the MS and hippocampus for the full 6 min sessions are shown in supplemental material (Supp. Fig. 3). An illustration of the mean amplitude within the theta band for the MS and hippocampus for the 6 mins of Y and B stimulation are shown in Fig. 2B while the microcircuit level mechanism by which optical stimulation of the MS influences hippocampal oscillations is provided in Fig. 2C-D. The results of GEE analysis of changes induced by B stimulation to the theta band properties of representative LFP signals from the hippocampus and MS of three animals are shown in Fig.3A. Mean peak theta frequency decreased significantly between Y (6.4 ± 0.0 Hz) and B (6.0 ± 0.09 Hz) stimulation epochs ($p < 0.0001$), indicating a shift in peak hippocampal theta oscillations to the septal input frequency. Meanwhile, no significant changes were found relative to Y or B

stimulation for hippocampal mean peak theta amplitude or mean normalized theta amplitude. In contrast, significant changes to both theta amplitude and frequency in the MS were caused by B stimulation (Fig. 3B). Mean peak theta frequency increased significantly between Y (5.3 ± 0.22 Hz) and B (6.0 ± 0.0 Hz) stimulation epochs ($p = 0.001$), indicating a universal shift in peak hippocampal theta frequency in correspondence with the artificial theta band stimulation. B stimulation also caused significant increases in mean peak theta amplitude of the septal signal ($p < 0.0001$), as well as significant increases in mean normalized theta amplitude ($p < 0.0001$). The combined MS peak theta frequency and amplitude per animal and stimulation condition are shown in supplemental material (Supp. Fig. 3). Non-selective optogenetic stimulation of the MS therefore supersedes endogenous hippocampal theta oscillations while the rats have limited mobility.

MS optical stimulation aligns septal and local theta phase preference of hippocampal neurons

The effect of stimulation condition on theta phase preference of CA1 pyramidal cells (n= 64), pooled for all 3 animals (n= 33, 14 and 17), is shown in Fig. 3C. Significant mean resultant vector lengths (RBAR) and phase angles were found for the pyramidal cell population in Y and B stimulation conditions referenced to local theta band signals from the hippocampus (0.679 at 66° vs. 0.761 at 14°) and MS (0.355 at 355° vs. 0.539 at 28°). Watson-Williams test reveals that these phase preferences were significantly different relative to both hippocampal ($p < 0.0001$) and MS ($p= 0.027$) theta phase. Paired t-test comparisons for the RBAR values for all individual cells by reference region and condition demonstrate that B stimulation had no effect on the average length of the resultant phase vector relative to local hippocampal theta ($p=0.115$) but did have a significant effect relative to septal theta ($p < 0.0001$). Taken together, these analyses show B stimulation causes a significant increase in the degree of subcortical influence exerted over hippocampal theta properties at both the level of the LFP as well as the level of cell interaction with the LFP as measured by CA1 pyramidal cell phase preference. B MS stimulation caused an alignment of preferred theta angle of CA neuronal firing activity toward the theta trough of both septal and hippocampal references. Ultimately, septal projections have a stronger influence over the timing of CA1 neuronal action potentials during B stimulation than during baseline Y stimulation. This doesn't perturb the strength of their modulation by the local hippocampal synaptic inputs but it does suggest that the MS is dictating the preferred theta phase of firing in reference to these inputs.

MS optical stimulation entrains burst timing of a subset of pyramidal cells

Through the analysis of autocorrelograms (ACGs) we determined the inter-spike intervals of CA1 pyramidal cells to examine the influence of artificial theta stimulation protocols on the temporal organization of complex bursts. Despite robust entrainment of the LFP and phase preference,

only 25% of recorded cells were found to have altered temporal firing patterns between Y and B stimulation, as determined by modulation depth and inter-spike interval frequency. Example autocorrelation histograms of this stimulation responsive subset of pyramidal cells as well as representative interneurons are shown in Fig. 3E-F. GEE analysis revealed that in comparison to Y stimulation, the upper 25% of the most B stimulation responsive pyramidal cells (U25MD Supp. Fig. 5) exhibited a significant increase in modulation depth ($p < 0.0001$) and a decrease in modulation frequency toward 6 Hz ($p < 0.0001$). Modulation depth of the remaining 75% of the cells (R75MD in Supp. Fig. 5) significantly worsened in response to B stimulation ($p < 0.0001$) while the modulation frequency increased significantly. However, as our method of ACG analysis tended to over-estimate periodicity when modulation depth was low, this increase in frequency was likely an artifact of decreased modulation depth. Finally, the U25MD cells have a significantly higher overall mean firing rate during baseline than the R75MD cells ($p=0.032$). Importantly, B stimulation did not cause changes in the overall mean firing rate in either cell population (U25MD or R75MD) relative to baseline ($p = 0.224$).

The main result of this experiment is that optical stimulation while at rest not only influences theta frequency of synaptic oscillations, but it also affects the local burst timing patterns ~ ¼ of recorded neurons. The results also indicate that cells that were most active prior to stimulation were more likely to be entrained by MS stimulation while cells that were less active prior to stimulation were more likely to exhibit attenuated temporal modulation. Therefore, artificial theta stimulation may interact with recent cell activity to recruit active cell assemblies.

Experiment 2

MS entrainment of hippocampal LFP theta band oscillations is task conditional

In order to examine the influence of changes in cognitive demand on both the temporal dynamics of the septo-hippocampal circuit as well as the efficacy of its entrainment by artificial theta stimulation, we conducted a 2nd experiment that behaviorally titrated hippocampal dependence during 6 Hz Y and B MS stimulations. Animal speed has an important effect on theta band properties [39] and prior studies have described optogenetic lateral septum stimulation effects on movement speed [50], GEE analysis revealed no main effect of stimulation and task condition on mean animal speed (YC = 14.03 ± 1.63 cm/s; YUC = 11.63 ± 1.35 cm/s; BC = 12.63 ± 1.46 cm/s; BUC = 10.69 ± 1.24 cm/s; $p = 0.393$). Examples of speed-sorted spectrograms of an experimental series including all 4 sessions can be found in Supp. Fig. 6.

An illustration of the relationship between movement speed and theta band properties of frequency and amplitude, in both the hippocampus and MS, during each stimulation and task condition is shown in Fig. 4A-B. In both structures, Y stimulation in each task condition (cued and uncued) produced an expected result where theta amplitude and frequency are increased relative

to slower movement speeds. Similar to the result of a previous report [34], we found that B stimulation during the cued condition at movement speeds ≥ 5 cm/s caused a bisection of the theta band. Theta frequency toggled between the 6 Hz septal input frequency and an endogenous theta frequency at approximately 9 Hz. During slower movement speeds ≤ 2 cm/s, the hippocampal theta frequency predominately oscillated at 6 Hz. When theta cycles are plotted for all speeds, it is apparent that theta frequency during BC still increases with movement speed but is shifted approximately 1.5 Hz faster than baseline conditions in YC. Speed sorted spectrograms for each of these example sessions are in supplementary material (Supp. Fig. 6). The endogenous hippocampal theta increased frequency with movement speed while simultaneously toggling back to the slower septal input frequency. Remarkably, this endogenous oscillation is weaker during BUC, resulting in a predominant theta oscillation frequency at 6 Hz regardless of movement speed (Fig. 4 B).

Across animals, GEE analysis found a significant main effect of task/stimulation condition with regard to mean peak theta frequency at speeds ≥ 5 cm/s ($p < 0.0001$). Specifically, mean peak theta frequency during BC was significantly faster than during BUC ($p=0.027$) and YC ($p=0.003$) (Fig. 4C). As shown by the example in Fig. 4A, this increase in endogenous peak theta frequency during BC serves to maintain a linear speed/theta frequency relationship. In contrast, endogenous theta was unable to compensate during BUC, exhibiting a mean peak theta frequency near the septal input frequency at 6 Hz. A significant main effect of condition was also found for mean peak theta frequency at movement speeds ≤ 2 cm/s ($p < 0.0001$), where mean peak theta in BC and BUC conditions were significantly lower than baseline conditions during YC ($p < 0.0001$ in both cases). Task conditional entrainment of mean peak theta frequency was not found at slow movement speeds when comparing BC and BUC ($p = 0.80$).

A significant main effect of stimulation/task condition was found across animals for mean peak amplitude during movement speeds ≥ 5 cm/s ($p = 0.004$). Specifically, mean peak theta amplitude was reduced in both BC ($p < 0.0001$) and BUC ($p = 0.009$) in comparison to baseline conditions. In contrast, we did not find a significant main effect of condition for mean peak theta amplitude during movement speeds ≤ 2cm/s. Direct comparison of the mean peak theta amplitude in each stimulation/task condition at fast or slow speeds by paired t-tests revealed that amplitude was greater when moving ≥ 5cm/s than ≤ 2 cm/s during YC ($p =0.027$) and YUC ($p =0.044$). However, this speed relationship was disrupted during BC (89.04 ± 0.782 vs. 92.13 ± 1.79; $p =0.118$) and BUC (90.25 ± 2.03 vs. 92.72 ± 2.58; $p = 0.071$), largely due to the alteration of the distribution of power throughout the theta band during B stimulation when moving ≥ 5cm/s. An indication that this interpretation is correct is suggested by GEE analysis of the normalized mean theta amplitude, unfiltered with regard to speed. Importantly, no main effect of stimulation/task condition occurred. This further implies that peak amplitude reductions during BC

and BUC (Fig. 4C) were a result of compensatory endogenous theta signals that distributed the power of hippocampal theta between endogenous and artificial theta. Similarly, we used GEE analysis for mean theta frequency for each stimulation/task condition, again unfiltered relative to speed. A significant main effect of condition was found ($p = 0.042$) where the mean theta frequency during BC was not significantly different from baseline during YC. However, mean theta frequency was significantly lower during BUC than BC ($p = 0.006$). Frequency and amplitude shifts during BC have the ultimate effect of moving the theta signal back to the mean. This reversion to the mean was less likely to occur during BUC due to the attenuation of the endogenous theta signal at 9 Hz (Fig. 4C).

Applying the same GEE approach to theta band properties in the MS (Fig. 4D), there was a significant main effect of stimulation/task condition for mean theta frequency when movement speed was unfiltered ($p < 0.0001$). In this case, while there was no difference between mean theta frequency during BC and BUC, there was a significant difference between BUC and baseline conditions in YC and YUC ($p < 0.0001$) indicating a significant decrease in mean theta frequency during B stimulation at 6 Hz. Analyses with and without speed filters demonstrated a clear increase in signal amplitude during B stimulation relative to YC and YUC ($p < 0.0001$). There was no significant task effect for theta signal amplitude during BC and BUC.

Finally, GEE analysis was used to test for the effect of task/stimulation conditions on the linear relationship between speed/theta frequency. In accordance with the example shown in Fig. 4 A, a significant main effect of condition was found ($p < 0.0001$) where speed and theta frequency correlations increased significantly between YC and YUC ($p < 0.0001$). This suggests network level changes in response to increased cognitive demands during the uncued spatial accuracy task. In line with the maintained speed/theta frequency relationship in spite of regular toggling back to the septal input frequency (Fig.4A), speed/theta correlations across animals during BC are similar to YC. In contrast, speed/theta correlations are significantly reduced during BUC in comparison to BC ($p = 0.001$) and YUC ($p < 0.0001$). This further indicates that task demands during BUC change network dynamics in a manner that makes endogenous compensation for the septal input frequency at 6 Hz more difficult. A significant main effect of condition was present with regard to speed/theta frequency in the MS, ($p < 0.0001$) where speed/theta correlations were abolished during B stimulation and were significantly lower during BUC than YC ($p = 0.001$) or YUC ($p < 0.0001$).

While the majority of this report focuses on 6 Hz stimulation of the MS, we also carried out a more limited series of experiments using 10 Hz stimulation in the same animals (Supp. Fig. 7). The mean and standard errors of the same variables described in the 6 Hz stimulation analyses are reported in Supp. Table 1. In brief, during BC there was a tendency of the hippocampal theta signal to shift toward the endogenous theta mean at movement speeds greater than 20 cm/s

(Supp. Fig. 7A). This led to an inversion of the speed/theta frequency correlation. As was the case with 6 Hz stimulation experiments, this competition with endogenous theta was largely absent during BUC (Supp. Fig. 7B). However, across animals, this task conditional efficacy of 10 Hz entrainment was not found to be statistically significant. Both peak and mean theta frequency during BC and BUC conditions tended to resemble the septal input frequency more than endogenous theta. Therefore, if the reversion to theta mean during BC was a form of network compensation, it may be more difficult for the network to compensate for stimulation frequencies further from the mean.

Finally, hippocampal LFP recordings were made from an additional 3 animals that foraged for pellets in the open field (Supp. Fig. 8). Speed/theta frequency correlations were on par with YC in the previous experiment, where recordings were carried out in the absence of hippocampus-dependent cognitive demand (Supp. Table 2). In addition, there were no significant differences in speed/theta frequency or other theta property variables between 2 different exposures to the open field. This speed/theta frequency stability implies that the significant increases found between YC and YUC in the previous experiment were not an effect of re-introduction to the arena and were more likely a consequence of hippocampus-dependent cognitive demand.

We have therefore shown that optogenetic stimulation of the MS supersedes synaptic hippocampal oscillations when the animals are moving slowly or at rest in both experiments 1 and 2. Remarkably, entrainment of hippocampal theta oscillations during faster movements is task conditional and strongly suggests altered microcircuit dynamics in the septo-hippocampal circuit during performance of the uncued rather than the cued spatial accuracy task.

MS entrainment of theta phase preference reveals a temporally ordered hierarchy of hippocampal inputs

As task demands have previously been shown to alter phase preference of CA1action potentials that may reflect how information is processed in neural circuits [30], we asked how changes in cognitive demand in cued and uncued spatial accuracy may lead to changes in CA1 temporal processing relative to local theta oscillations as well as the theta pacemaker in MS. In addition, we asked how these putative changes were influenced by B stimulation of the MS.

In all 4 simulation/task conditions we calculated the mean angle and magnitude of phase preference relative to both hippocampus and MS theta as determined by the resultant vector lengths of individual cells (n=166) as well as for cell population ensembles (Fig. 5) from each of the 3 animals (n= 22, 57, and 87). An example of these analyses using circular statistics in 1 animal is illustrated in Fig. 5A-B as well as in the form of mean firing probability of all cells for each 30° bin of theta in Supp. Fig. 9(A-B). GEE analysis of the length of the resultant phase vectors (RBAR) for the cell populations referenced to *hippocampal theta* in each animal (Fig. 5C)

found a significant effect of stimulation/task condition ($p < 0.0001$). There was no change in RBAR between YC and YUC ($p = 0.194$), although the mean angle of the resultant vector tended to move backwards during YUC (38.33 ± 12.47°). A significant reduction in mean RBAR was found across animals between YC and BUC as well as YUC and BUC ($p < 0.0001$). However, RBAR during BC was more variable between animals and, while only marginally different from BUC ($p = 0.053$), was also similar to YC. A complementary analysis of population level dispersion (Fig. 5D) found a significant main effect of stimulation/task condition ($p < 0.0001$). Again, while YC and YUC had similarly low levels of dispersion, there was a significant increase in dispersion levels during BUC ($p < 0.0001$) in comparisons to both YC and YUC. Taken together, these analyses show a universal reduction in the temporal organization of hippocampal neurons relative to local theta oscillations during BUC. During BC, population level phasic organization of neurons relative to local theta is neither as high as baseline levels during YC nor as low as during BUC.

When the same cells are referenced to MS theta (Fig. 5D) there was no significant main effect of stimulation/task condition for either the length of the resultant phase vector ($p = 0.717$) or dispersion ($p = 0.101$). This is another indication that the artificial theta signal supersedes endogenous theta during B MS stimulation. However, there was a significant stimulation effect ($p = 0.016$) on preferred phase angle between YC and BC (MSYC-MSBC = 90 ± 33.35°) in comparison to YUC and BUC (MSYUC-MSBUC = 161 ± 20.42°). Septal phase shifts during B stimulation were significantly more pronounced and less variable during uncued sessions than cued sessions when compared to Y stimulation sessions. Finally, we compared baseline preferred phase angle of hippocampal theta during baseline to septal theta during baseline in the uncued task (HCYUC - MSYUC = 191.00 ± 29.67°) as well as to septal theta references during B stimulation in the uncued task (HCYUC - MSBUC = 41.33 ± 31.13°). The septal and hippocampal theta signals during the uncued task drove hippocampal cell activity at opposite phases. B stimulation caused an approximately 180° shift in the septal theta phase preference ($p = 0.006$). The results of this experiment strongly imply that the artificial theta stimulation competes for control over the phasic firing of hippocampal neurons and supersedes endogenous theta oscillations during BUC, potentially by occupying the same preferred phase vector.

In order to further test the influence of cognitive demand on phase preference, we recorded cells ($N = 158$) during a foraging task with 3 animals ($n = 62$, 29 and 67) and analyzed spike activity relative to local hippocampal theta oscillations (Supp. Fig. 9C-D). Circular statistics from the pooled cell population revealed a significant resultant vector ($p = 0.01$) with a mean direction of 213°. This angle is similar to the example shown in Fig. 5A during YUC and may denote a default phase vector angle during hippocampal independent tasks. Moreover, this result suggests that the increased mean resultant phase vector length during YUC may serve as a network level biomarker of increased cognitive demand.

Taken together, these results strongly suggest a temporally ordered hierarchy among projections to hippocampal synapses. These synapses likely compete to drive hippocampal neurons at phases of theta that reflect the facilitation of specific synapses that underpin either sensory processing, active navigation, or the recall of the goal zone location.

MS entrainment of burst timing mirrors task conditional entrainment of LFPs and reveals a subpopulation of cells driven by septal inputs

As a complementary measure of the effects of task and stimulation conditions on temporal coding, we applied the same GEE methodology to the results of autocorrelogram analyses. This was done in order to test for stimulation/task conditions (Fig. 6A) on the timing intervals of spike trains from CA1 pyramidal cells (n= 144) from 3 animals (n= 23, 64 and 57). As this analysis was sensitive to rate changes, we first analyzed for any main effect of mean overall rate by stimulation/task conditions. Although there was a decrease in mean overall rate during YUC, rate was not significantly different between baseline conditions in comparison to B stimulation during cued sessions or uncued sessions. Stimulation did not alter overall mean firing rate.

GEE analysis revealed a significant main effect of pyramidal cell modulation depth (Fig. 6B) by condition ($p < 0.0001$). The modulation depth was lowest during BUC (Fig. 6B) and significantly different from all other sessions ($p < 0.0001$). BC was also significantly different from YC ($p < 0.0001$) while YC and YUC were not significantly different ($p = 0.350$). Using modulation depth as a covariate, GEE factorial analysis found a significant effect of stimulation/task condition (Fig. 6C) across animals ($p = 0.007$) where BUC was significantly reduced in comparison to YC ($p = 0.023$), YUC ($p = 0.04$) and BC ($p = 0.01$). Remarkably, this result is similar to stimulation/task effects on mean theta frequency (Fig. 4C) where the endogenous theta frequency is unable to compensate for the MS stimulation during BUC. Modulation frequency measurements also exhibited a significant interaction of stimulation/task condition with modulation depth ($p < 0.0001$), where all sessions were significantly different from BUC ($p < 0.01$). In order to understand this interaction, modulation frequency histograms for all recorded cells in each stimulation/task condition were constructed (Fig. 6D). As noted previously [31], the inter-spike interval periodicity during baseline conditions for many of the cells was ~ 1 Hz ahead of the mean theta frequency. This distribution is unaffected by task demands in the cued or uncued sessions. However, during B stimulation this distribution was dramatically altered. The frequency distribution became more normal during BC and became bimodal during BUC. As our ACG analysis had the tendency to overestimate frequency when modulation depth was low, and there was a significant interaction between modulation depth and modulation frequency, we further examined the relationship between these 2 variables in a scatterplot for all cells (Fig. 6E). The plots re-iterate the LFP results of previous analyses during the BC condition and demonstrate the bisection of the cell population at the level of spike-timing within bursts. Many of the cells are entrained at the septal

input frequency while others are more responsive to the endogenous theta signal. During BUC, the majority of the cells that exhibited a modulation frequency greater than 7.5 Hz also present an attenuated modulation depth. Meanwhile, cells with a modulation frequency less than 7.5 Hz do not experience the same loss of modulation.

In response to this observation, we conducted an additional test for modulation depth for all cells during BC and BUC. Cells were separated into 2 populations by modulation frequency, either ≥ 9 Hz or < 9 Hz (Fig. 6B inset). We chose this frequency based on the results of Fig. 6D-E, where the 2 populations appear to separate. During BC, cells with a modulation frequency < 9Hz (38%, Mean = 0.00828 ± 0.0010) were compared to cells with a modulation frequency > 9 Hz (62%; Mean = 0.00518 ± 0.00058) by one-way analysis of variance. Cells with a modulation frequency < 9 Hz were found to be significantly more modulated than those ≥ 9 Hz ($p = 0.005$). Although all cells were less modulated during BUC, the modulation pattern was repeated. An additional one-way analysis of variance found that cells with a modulation frequency < 9Hz (31%, Mean = 0.00607 ± 0.0008) were again significantly more modulated ($p < 0.0001$) than cells with a modulation frequency > 9 Hz (69%; Mean = 0.00199 ± 0.00025). During BUC then, cells that were modulated near the septal input frequency retained temporal modulation while those that were modulated by endogenous theta were no longer temporally organized. This result therefore revealed a subpopulation of approximately 1/3 of the recorded cell population that was more responsive to septal inputs than local theta oscillations.

As in experiment 1, cells with modulation frequency either ≥ 9 Hz or < 9 Hz during BC were traced back to the YC session to determine if their baseline mean firing rates were higher than the cells with a periodicity at a faster rate. Unlike the results during the flowerpot recordings, in this case mean firing rate was not the delineating factor between stimulation responsive cells and the remainder of the cell population (1.21 ± 0.144 Hz vs. 1.29 ± 0.13 Hz; $p = 0.719$).

We have shown a close correspondence between both the burst-timing properties of hippocampal neurons and synaptic oscillations at theta timescale. At both levels, the efficacy of entrainment at the septal input frequency was task dependent. The same proportion of cells in the cued and uncued sessions responded robustly to B stimulation. Unlike experiment 1, these cells were not more active than other cells during baseline, suggesting a more complex interaction with active navigation.

Stimulation induced changes to LFPs and the temporal organization of spike-timing do not alter place cell firing fields

As we found significant stimulation/task induced alterations in the temporal organization of hippocampal pyramidal cells, we asked if these changes influenced the spatial firing of place cell

firing fields. A total of 103 cells met criteria for place cell analyses from 3 rats (n = 18, 44 and 41). Examples of several simultaneously recorded place cell firing fields across stimulation/task conditions are shown in Fig. 7A. As summarized in Fig. 7B, GEE analysis found no significant main effect of stimulation/task conditions for mean field coherence, mean overall firing rate, mean firing field stability, mean field size, mean in-field firing rate, and mean out-field firing rate. We therefore conclude, in accordance with previous studies, that perturbations of hippocampal theta oscillations through local septal manipulation or through systemic pharmacological intervention do not interfere with the spatial firing of hippocampal place cells [28, 51]. Although the temporal organization of cell activity has been altered by septal stimulation, the spatial code remains intact.

Superseding endogenous theta oscillations affects spatial accuracy in the uncued task

We have shown that MS stimulation affects the endogenous LFP theta band, theta phase preference and the inter-spike interval of pyramidal cell action potentials, yet spares the spatial tuning of hippocampal place cells. While the spatial code in the hippocampus is maintained, cell activity during BUC is dissociated from local, endogenous theta. We therefore ask if the temporal organization of hippocampal cells relative to local, endogenous theta oscillations is necessary for self-localization metric relative to a goal zone in the uncued spatial accuracy task. For each of the 3 animals, the series of stimulation/task conditions (YC, YUC, BC and BUC) was repeated 4 times on different days. However, for 1 rat one of these series was excluded from analysis as the rat failed to participate in either the YUC or BUC condition although its behavior on the other days was similar to the other 2 rats. Examples of behavioral performance for each animal in each stimulation/task condition are shown in Fig. 8A-C. Further examples of path and search pattern accuracy relative to the goal zone can be found in supplementary material (Supp. Fig. 10).

Across animals, GEE analysis found a significant main effect of stimulation/task condition for mean number of rewards ($p < 0.0001$). The lowest mean number of rewards was accrued during BUC sessions (Fig. 8D), which was significantly different from both YC and BC ($p < 0.0001$) and from YUC ($p = 0.036$). While the mean number of rewards between YC and BC were similar, the mean number of rewards during YC was significantly greater than during YUC ($p < 0.0001$). In contrast, no significant main effect of stimulation/task condition for mean number of goal entrances was detected. Taken together, these results imply that the uncued version of the task was more challenging for the animals. This was particularly evident during BUC, where the animals performed significantly worse than YUC but made a similar number of goal entrances without triggering reward. Put simply, the rats became more likely to overshoot the goal zone (Interaction between mean number of entrances and number of rewards between YUC and BUC; $p = 0.044$).

GEE analysis was also applied toward the mean accuracy of the goal search pattern in both the X and Y axes. A significant main effect of condition was found for X axis accuracy ($p < 0.0001$).

This difference indicated a difference between cued and uncued sessions and not of stimulation . In contrast, a significant main effect of condition ocurred for Y axis search accuracy ($p < 0.0001$). While there was no significant difference between YC and BC sessions, the mean distance between the center of the goal zone and the goal search pattern was significantly greater during BUC than YUC ($p = 0.03$). Therefore, the rats had a broader search pattern that began further from the goal zone. That this accuracy effect was detectable in the Y axis rather than the X axis suggests that the rats may have been able to use the proximity of the wall at the right edge of the goal zone as a spatial cue. When the rats moved further from the wall they may have been more likely to search an average of 5.24 pixels (~ 2 cm) further away from the goal than during YUC.

We conclude that while the rats were able to perform the uncued spatial accuracy task during the BUC condition, their performance was measurably worse than baseline conditions during the YUC condition in terms of both the reduced number of rewards and diminished spatial accuracy. Moreover, these results suggest that it may be possible to separate the septo-hippocampal functions of spatial metric from memory as alterations of temporal coordination primarily affect position estimates relative to a goal. Endogenous theta oscillations may therefore be necessary for the integration of distance, time and velocity in service of self-localization metric.

Discussion

We investigated how septo-hippocampal circuit state influenced the entrainment efficacy of both hippocampal local field potentials and single cell activity via nonselective optogenetic stimulation of the MS in wild-type rats. We accomplished this by making electrophysiological recordings while titrating the septo-hippocampal state between three contexts, when the animals were at rest or performing either a hippocampus-independent or hippocampus-dependent spatial accuracy task. We found that the entrainment of local field potentials and cell activity at the 6 Hz septal input frequency was more likely to supplant endogenous theta oscillations when the animal was at rest or performing the hippocampus-dependent, uncued version of the spatial accuracy task. Similar to findings in a previous report that involved septal stimulation while foraging for food pellets [34], septal stimulation during the hippocampus-independent task revealed complex interactions between the septal pacemaker and local theta inputs. This interaction may represent competing influences between artificial and endogenous theta oscillations over both synaptic current and the burst-timing of action potentials. During the hippocampus-independent, cued version of the task, hippocampal frequencies were more likely to match septal input frequency at 6 Hz during movement speeds $\leq$ 2 cm/s. However, hippocampal frequency 'toggled' between 6 Hz and an endogenous theta frequency at ~ 9 Hz during movement speeds $\geq$ 5 cm/s. Displacing theta frequency 1.5 Hz down from the mean baseline theta frequency of 7.5 Hz during MS stimulation therefore results in an endogenous theta frequency 1.5 Hz up from the mean to ~ 9 Hz. Remarkably, the endogenous signal still increased linearly with speed. We therefore hypothesize

that this endogenous signal is compensatory as it ultimately served to maintain a linear relationship between theta frequency and animal speed. The maintenance of theta's dynamic relationship to the animal's behavior at another part of the theta band raises the possibility that the endogenous signal may actively 'error-correct' in response to frequency stimulations that are out of register with intrinsic speed and position estimates.

Endogenous hippocampal theta involves the complex interplay of input from two major structures, the MS and the entorhinal cortex. While the MS has a critical role in the rhythmic pacing of hippocampal theta [7, 8, 31], complementary inputs from the entorhinal cortex, itself influenced by projections from the MS [52], are also important for generation of theta oscillations. Locomotion speed signals computed in the MS are transmitted to the entorhinal cortex via glutamatergic axonal projections [53]. It is possible to dissociate the linear speed relationship of both cell firing rate and local theta frequency in the entorhinal cortex, where only the speed relationship with theta frequency is weakened following inactivation of the MS (Hinman et al, 2016). It is therefore possible that the entorhinal cortex, with an internal metric supplied by grid cell firing rate [54], could project a separate speed signal, to the hippocampus that is independent of the MS. In this manner, the entorhinal cortex may act as an error-corrector [55] in the speed and distance calculation during stimulation in the cued version of the task.

Hippocampal LFP entrainment at 6 Hz was more evident in flowerpot and uncued contexts, as well as the cued context during slow movement speeds. This therefore suggests that subcortical projections are more influential at hippocampal synapses while at rest and during active navigation in a hippocampal dependent spatial task. Increased competition with endogenous theta oscillations during faster movements in the hippocampal independent cued task or foraging [34] , in the absence of cognitive demand, demonstrates a default dominance of cortical movement during fast speeds that may denote increased sensory processing. Yet during increased cognitive demand during the uncued sessions, OLM interneurons may be more engaged through elevated acetylcholine from septal projections. This could increase inhibitory tone at sensory inputs from entorhinal projections at the apical dendrite while facilitating the transmission of intrahippocampal information from CA3 by inhibiting interneurons in stratum radiatum [56]. If the compensatory endogenous signal did originate from the entorhinal cortex, OLM inhibition of entorhinal projections at CA1 synapses could make the relationship between septal input and local synaptic oscillations more linear.

Analysis of the temporal intervals in the burst spiking patterns of CA1 pyramidal cells mirrored this competition between local and septal theta oscillations during the cued version of the task where cells tended to separate between two populations, with inter-spike intervals at approximately 6 or 9 Hz. During the uncued task, burst spiking patterns of a subset of cells were modulated at 6 Hz while temporal modulation of the remaining cells was significantly attenuated,

again mirroring the dominance of artificial septal theta oscillations in the LFP. This finding provokes the question of whether the cells that are more responsive to the 6 Hz stimulation are somehow hardwired to respond to subcortical inputs or if local signals are somehow delegating which cells fall into which population. In contrast, in the case of the flowerpot recordings, determining the nature of the responsive cells was rather straightforward. Cells that had been most active in the 6 min period prior to B stimulation were more likely to exhibit temporal modulation at a periodicity matching the frequency of septal input. Baseline firing rate did not play a role in the recruitment of stimulation responsive cells during the hippocampus-independent spatial accuracy task.

Optogenetic stimulation of parvalbumin positive interneurons in the MS of transgenic mice was recently found to pace hippocampal theta frequencies at 10 or 12 Hz stimulation frequencies [31]. The stimulation led to the scaling of burst timing rhythmicity of 25-30 % of pyramidal neurons within 1 Hz of the stimulation frequency. This is similar to our findings where in all 3 contexts (flowerpot, cued accuracy and uncued accuracy) ~ 30% of the recorded cells exhibited burst timing periodicity that was similar to the B simulation frequency at 6 Hz. In addition, while the Zutshi et al. study did not find changes to phase preference or the resultant length of the phase vector, the cells no longer showed a consistent relationship with endogenous theta, as determined by the attenuation of the slope of place cell phase precession. This is also similar to our findings during the hippocampus-dependent task when B stimulation was more likely to supersede endogenous theta oscillations. During B stimulation in the uncued task, the majority of the cells with modulation frequency greater than 8 Hz were found to have a significantly attenuated temporal modulation. Therefore, performing a version of the accuracy task that increased cognitive demand was sufficient to significantly attenuate the compensatory response of endogenous theta and increase the probability that hippocampal theta frequency will match septal input, regardless of movement speed. This suggests septal projections have a significantly stronger influence over local theta oscillations in this context. Whether this is a feature of increased subcortical input to the hippocampus or a feature of alterations at local synapses is key to understanding the mechanism by which active cognition affects the efficacy of entrainment in the septal-hippocampal circuit.

The results of phase preference analyses in the uncued task indicated that the resultant population vector lengths were significantly diminished relative to local theta but were sustained relative to septal theta, albeit at a different phase. The default phase vectors of hippocampal cells relative to septal and hippocampal theta references were approximately 180° apart. During B stimulation in the hippocampus-dependent task, the resultant septal vector shifted 180° to occupy a similar phase space as the local hippocampal vector during control stimulation. The septal phase preference difference between Y and B stimulation is particularly evident during B

stimulation in the uncued spatial accuracy task. Across animals, this result suggests a phase ordered hierarchy of hippocampal inputs where the artificial theta signal from the MS is more likely to supersede endogenous hippocampal theta in the same phase vector during active navigation toward a goal.

Stimulation frequency, as well as task condition, may be important variables with regard to entrainment efficacy. Although some endogenous compensation was found during 10 Hz stimulation frequency in the cued version of the task, where peak frequency shifted down toward mean baseline theta frequency, it was not sufficient to cause a significant main effect of task condition. Nonetheless, excellent control of theta oscillation frequency was found across animals during 10 Hz stimulation in the uncued spatial accuracy task, without the use of cell type specific optogenetic stimulation. Although response to stimulation by each septal cell type was not measured in this study, it is unclear whether or not the simultaneous stimulation of GABAergic and glutamatergic cells in the MS occurred. However, it is clear from the results that the resultant septal oscillations generated the prerequisite artificial theta patterns that were necessary for the experiment (i.e., 6 and 10 Hz theta oscillations). Selective stimulation of mouse septal GABAergic cells [31] and glutamatergic cells [13, 32] lead to excellent control of hippocampal oscillations at most frequencies within the theta band. Stimulation of glutamatergic axon terminals in the hippocampus, however, do not alter theta frequency [32]. This finding supports the notion of an intraseptal tuning mechanism where septal glutamatergic neurons initiate synchronization with GABAergic neurons, and to a lesser extent cholinergic neurons, to pace hippocampal theta. Therefore, even if both cell types were simultaneously activated, they would still fire synchronously. Ultimately the activation of septal GABAergic interneurons alone may be sufficient to pace theta due to their unique connectivity with hippocampal GABAergic interneurons and their tendency to phase-lock to theta [7-9, 11, 14, 57]. Septal cholinergic neurons, due to their contrasting temporal dynamics, are less likely to fire at the same time as GABAergic and glutamatergic neurons in response to stimulation [58] and are thought to be more involved with signal amplitude in theta range rather than pacing theta frequency [59, 60]. Septal cholinergic neurons have also been hypothesized to be involved with the linear relationship between speed and theta amplitude [31]. In accordance with our results we therefore propose that non-selective optogentics in tandem with experiments utilizing cell type specific simulation and titration of behavior comprise an important approach to deconstructing the neural circuits that underpin pacing of the hippocampal network.

An important question we wished to address in the current study was whether the interference with endogenous temporal discoordination of CA1 hippocampal neurons caused by optogenetic stimulation would cause deficits in the performance of a spatial task. This question is largely driven by previous findings where a lack of temporal organization in CA1 place cells relative to

local theta oscillations was found to correlate with poor cognitive outcomes in animals that had experienced febrile status epilepticus in early life [30]. Inactivation of the MS leads to a significant loss of theta oscillations in the hippocampus and alterations in the spacing of entorhinal grid cells [52, 61] though the hippocampus is still able to remap and form new and stable spatial representations in new environments in the absence of intrinsic theta, [51]. This is in accordance with our findings where manipulating endogenous theta oscillations through optical stimulation of the MS was not found to affect firing field properties in either version of the spatial accuracy task, despite the task differences in relation to hippocampal LFP entrainment and burst-timing dynamics. Apart from the independence of the hippocampal spatial code from theta oscillations, a handful of experiments have illustrated the necessity of the phasic organization of hippocampal neurons with regard to learning and memory [28-30, 62, 63]. A substantial literature has also developed in relation to the use of electrical pulses in the MS for artificial theta stimulation (ATS) of the hippocampus. This technique has been used as a type of neuroprosthetic meant to enhance learning and memory in disease models where intrinsic theta oscillations are compromised [64-67]. Importantly, this literature has shown variability in behavioral outcome measures. Modest degrees of improvement have been found in spatial working memory tasks using ATS protocols [65, 67], or theta burst stimulation protocols [66]. However, another study showed that while ATS restored hippocampal theta oscillations in fimbria fornix lesioned rats, this treatment was more likely to disrupt the encoding of contextual fear responses in these animals as well as sham lesioned controls [64]. This has led to the suggestion that ATS induced hippocampal theta may be more beneficial for working memory tasks than for encoding information [64]. Similarly, a recent study using ATS in epileptic animals found some restoration of hippocampal theta oscillations as well as improved behavioral performance on a spatial path integration task, but that the ATS protocol interfered with path integration in control animals [68]. Few papers have clearly shown the necessity of endogenous hippocampal theta oscillations for the performance of a spatial task. Lesioning of the MS [69] was shown to significantly interfere with the performance of a previously learned spatial task, on an elevated circular track where animals were able to at least recognize a goal location if they stumbled upon it, but otherwise had difficulty in determining goal location. Pharmacological inactivation of the MS was shown to interfere with learning a Morris water maze task [65], which was at least partly mitigated in early training sessions by artificial theta stimulation in the fimbria-fornix.

In our study, we have shown that MS stimulation during the uncued spatial accuracy task dissociates cells from endogenous theta in favor of a continuous, artificial theta signal. This result indicates that increased spatial processing demands allow the entrainment of the hippocampal network and concomitantly allows for an examination of the role that dynamic, endogenous theta plays with regard to the ability to self-localize relative to a goal location. In this context the hippocampal network is driven by an artificial theta signal but theta frequency no longer expands

and contracts in relation to speed. This manipulation should therefore interfere with theta's presumed role in the computation of position metric as distances correspond to proportional msec scale epochs within theta oscillations [25, 39, 70]. It also allows for the simultaneous examination of endogenous theta's role in the retrieval of task-associated memory [27].

Despite the observation that B stimulation significantly reduced the number of rewards during the uncued spatial accuracy task, it is important to note that the mean number of rewards was still above criterion levels. This suggests that even though the mean performance was measurably worse than performance during control stimulation in the uncued task, the rats remembered the goal location and how to perform the task. There are two ways of interpreting this finding. One is that endogenous theta is not necessary for the recall of goal location. The other is that the artificial theta oscillation is sufficient for supporting recall. Knowing which is the correct interpretation will require eliminating theta oscillations altogether during the uncued accuracy task.

What is clearly most affected by the stimulation was the rat's ability to accurately localize the goal zone. The rat's estimation of the goal zone location, as determined by where the rat slowed down prior to pausing, was consistently off by several centimeters. That this inaccuracy was found in the y-axis suggests that the rats became more imprecise the further they were from the arena wall. Given that the place cell spatial code was unaffected by B stimulation in either version of the accuracy task, these results suggest that dynamic endogenous theta frequency oscillations may be necessary for the integration of distance, time and velocity in service of reckoning self-localization metric. This interpretation of the data is supported by previous experiments that have shown that lesions of the medial entorhinal cortex or inactivation of the MS impaired the ability of the rats to estimate linear distances based on self-movement information [23]. The results of the Jacob et al. study indicated that theta oscillations in the septo-entorhrinal circuit, but not necessarily the hippocampus, were necessary for path integration and determining position in space. In light of our experimental results, endogenous theta oscillations can be thought to provide both temporal organization and an egocentric metric that translates synaptic strengths to perceived changes in allocentric position computations relative to spatial cues during movement and navigation [24].

We have shown that ongoing, dynamic theta oscillations can be reliably occluded by optogenetic stimulation of the MS, at any running speed, if the rats are actively engaged in the uncued version of the spatial accuracy task. This is yet further proof that the MS acts as a pacemaker for endogenous theta oscillations [7, 8, 31]. These results therefore serve a dual purpose. They provide important insights into the origins of complex oscillations in a circuit that is known to underpin spatial learning and memory. They also instruct us on how to interact with a dynamic circuit in a manner that leaves much of the circuit function, such as the firing of hippocampal

place cells, unaffected. The results also point out the importance of a critique recently levied against the field that asserts novel technical approaches in the study of neural circuits have been overly reductionist and have neglected behavior, the emergent property of coordinated neural networks [71]. In our study, behavior was not only a critical measure of the effects of 6 Hz optogenetic stimulation, but it also interacted with our electrophysiological measures. This interaction between stimulation and cognition has also been found in patients with epilepsy, where the effect of electrical stimulation in memory areas of the brain on the acquisition of word information during a verbal memory task was determined by current brain state [72]. If specific structures were determined to be in a low encoding state, stimulation improved acquisition. If already in a high encoding state, stimulation was detrimental to acquisition. Therefore, the efficacy of the stimulation may depend on the state of the stimulated circuit, which is also dictated by task demands. As mentioned above, this has been thought to play an important role in the variable results stimulation has had on learning and memory in both ATS protocols in rodents [64] as well as in human patients [73, 74]. Task demands and their influence on the interrogated circuit are therefore critical parameters to consider toward the design and interpretation of outcomes following brain stimulation. Although septal stimulation may improve learning in working memory tasks [34] it may interfere with performance on tasks where the endogenous signal is necessary for computing self-displacement and position in space [23].

Taken together, our results show that subcortical and cortical afferents to the hippocampus may compete at hippocampal synapses in a manner that is mediated by local microcircuits and cognitive demand. This competition is not only found at the level of synaptic current reflected in the frequency of LFP theta oscillations but also at the level of complex oscillatory patterns in CA1 pyramidal cell action potentials. Optogenetics not only has the potential to influence neural circuits, it can reveal changing dynamics in specific components of the circuit that underpin cognition. In this study, the key element for revealing these dynamics was the titration of cognitive demand in tasks that were behaviorally similar. This approach also showed that endogenous theta oscillations may be necessary for the integration of distance, time and velocity in service of self-localization metric. Disruption of the endogenous, dynamic theta frequency through frequency-fixed subcortical optogenetic stimulation may disrupt this metric. The results of the experiments therefore have important implications for understanding the circuit mechanisms by which electrophysiological signatures support cognition and for understanding how these circuits interact with stimulation. This reciprocal relationship between cognition, circuit state and entrainment efficacy is particularly important to consider as more studies begin to use optogenetic stimulation as a means of correcting circuit dysfunction in the hope of ameliorating cognitive deficits associated with temporal discoordination. Further studies toward this goal must carefully consider the potential beneficial or deleterious effects of optogenetic stimulation, as endogenous signals may be important to specific aspects of cognition.

References

1. Buzsáki G. Rhythms of the brain. Oxford ; New York: Oxford University Press; 2006. xiv, 448 p. p.
2. Grillner S. Neurobiological bases of rhythmic motor acts in vertebrates. Science. 1985;228(4696):143-9. PubMed PMID: 3975635.
3. Marder E, Calabrese RL. Principles of rhythmic motor pattern generation. Physiological reviews. 1996;76(3):687-717. doi: 10.1152/physrev.1996.76.3.687. PubMed PMID: 8757786.
4. Buzsaki G. Theta oscillations in the hippocampus. Neuron. 2002;33(3):325-40. PubMed PMID: 11832222.
5. Green JD, Maxwell D, Schindler W, Stumpf C. Rabbit EEG" theta" rhythm: its anatomical source and relation to activity in single neurons. J Neurophysiol. 1960;23(4):403-20.
6. Vanderwolf CH. Hippocampal electrical activity and voluntary movement in the rat. Electroencephalogr Clin Neurophysiol. 1969;26(4):407-18. PubMed PMID: 4183562.
7. Stewart M, Fox SE. Do septal neurons pace the hippocampal theta rhythm? Trends Neurosci. 1990;13(5):163-8. PubMed PMID: 1693232.
8. Stewart M, Fox SE. Firing relations of medial septal neurons to the hippocampal theta rhythm in urethane anesthetized rats. Exp Brain Res. 1989;77(3):507-16. PubMed PMID: 2806444.
9. Freund TF, Antal M. GABA-containing neurons in the septum control inhibitory interneurons in the hippocampus. Nature. 1988;336(6195):170-3. doi: 10.1038/336170a0. PubMed PMID: 3185735.
10. Gulyas AI, Gorcs TJ, Freund TF. Innervation of different peptide-containing neurons in the hippocampus by GABAergic septal afferents. Neuroscience. 1990;37(1):31-44. PubMed PMID: 1978740.
11. Hangya B, Borhegyi Z, Szilagyi N, Freund TF, Varga V. GABAergic neurons of the medial septum lead the hippocampal network during theta activity. J Neurosci. 2009;29(25):8094-102. doi: 10.1523/JNEUROSCI.5665-08.2009. PubMed PMID: 19553449.
12. Petsche H, Stumpf C, Gogolak G. [The significance of the rabbit's septum as a relay station between the midbrain and the hippocampus. I. The control of hippocampus arousal activity by the septum cells]. Electroencephalogr Clin Neurophysiol. 1962;14:202-11. PubMed PMID: 14038334.
13. Fuhrmann F, Justus D, Sosulina L, Kaneko H, Beutel T, Friedrichs D, et al. Locomotion, Theta Oscillations, and the Speed-Correlated Firing of Hippocampal Neurons Are Controlled by a Medial Septal Glutamatergic Circuit. Neuron. 2015;86(5):1253-64. doi: 10.1016/j.neuron.2015.05.001. PubMed PMID: 25982367.
14. Unal G, Crump MG, Viney TJ, Eltes T, Katona L, Klausberger T, et al. Spatio-temporal specialization of GABAergic septo-hippocampal neurons for rhythmic network activity. Brain Struct Funct. 2018;223(5):2409-32. doi: 10.1007/s00429-018-1626-0. PubMed PMID: 29500537.
15. Dragoi G, Carpi D, Recce M, Csicsvari J, Buzsaki G. Interactions between hippocampus and medial septum during sharp waves and theta oscillation in the behaving rat. J Neurosci. 1999;19(14):6191-9. PubMed PMID: 10407055.
16. Fox SE. Membrane potential and impedance changes in hippocampal pyramidal cells during theta rhythm. Exp Brain Res. 1989;77(2):283-94. PubMed PMID: 2792276.

17. Ylinen A, Soltesz I, Bragin A, Penttonen M, Sik A, Buzsaki G. Intracellular correlates of hippocampal theta rhythm in identified pyramidal cells, granule cells, and basket cells. Hippocampus. 1995;5(1):78-90. doi: 10.1002/hipo.450050110. PubMed PMID: 7787949.
18. Lubenov EV, Siapas AG. Hippocampal theta oscillations are travelling waves. Nature. 2009;459(7246):534-9. doi: 10.1038/nature08010. PubMed PMID: 19489117.
19. Mizuseki K, Sirota A, Pastalkova E, Buzsaki G. Theta oscillations provide temporal windows for local circuit computation in the entorhinal-hippocampal loop. Neuron. 2009;64(2):267-80. doi: 10.1016/j.neuron.2009.08.037. PubMed PMID: 19874793; PubMed Central PMCID: PMC2771122.
20. Hasselmo ME. What is the function of hippocampal theta rhythm?--Linking behavioral data to phasic properties of field potential and unit recording data. Hippocampus. 2005;15(7):936-49. doi: 10.1002/hipo.20116. PubMed PMID: 16158423.
21. Siegle JH, Wilson MA. Enhancement of encoding and retrieval functions through theta phase-specific manipulation of hippocampus. eLife. 2014;3:e03061. doi: 10.7554/eLife.03061. PubMed PMID: 25073927; PubMed Central PMCID: PMC4384761.
22. Hasselmo ME, Bodelon C, Wyble BP. A proposed function for hippocampal theta rhythm: separate phases of encoding and retrieval enhance reversal of prior learning. Neural computation. 2002;14(4):793-817. doi: 10.1162/089976602317318965. PubMed PMID: 11936962.
23. Jacob PY, Gordillo-Salas M, Facchini J, Poucet B, Save E, Sargolini F. Medial entorhinal cortex and medial septum contribute to self-motion-based linear distance estimation. Brain Struct Funct. 2017;222(6):2727-42. doi: 10.1007/s00429-017-1368-4. PubMed PMID: 28161726.
24. Buzsaki G. Theta rhythm of navigation: link between path integration and landmark navigation, episodic and semantic memory. Hippocampus. 2005;15(7):827-40. doi: 10.1002/hipo.20113. PubMed PMID: 16149082.
25. Buzsaki G, Llinas R. Space and time in the brain. Science. 2017;358(6362):482-5. doi: 10.1126/science.aan8869. PubMed PMID: 29074768.
26. McNaughton BL, Barnes CA, Gerrard JL, Gothard K, Jung MW, Knierim JJ, et al. Deciphering the hippocampal polyglot: the hippocampus as a path integration system. J Exp Biol. 1996;199(Pt 1):173-85. PubMed PMID: 8576689.
27. Hasselmo ME, Stern CE. Theta rhythm and the encoding and retrieval of space and time. Neuroimage. 2014;85 Pt 2:656-66. doi: 10.1016/j.neuroimage.2013.06.022. PubMed PMID: 23774394; PubMed Central PMCID: PMCPMC3918488.
28. Robbe D, Buzsaki G. Alteration of theta timescale dynamics of hippocampal place cells by a cannabinoid is associated with memory impairment. J Neurosci. 2009;29(40):12597-605. doi: 10.1523/JNEUROSCI.2407-09.2009. PubMed PMID: 19812334; PubMed Central PMCID: PMC2799373.
29. Bender AC, Luikart BW, Lenck-Santini PP. Cognitive Deficits Associated with Nav1.1 Alterations: Involvement of Neuronal Firing Dynamics and Oscillations. PLoS One. 2016;11(3):e0151538. doi: 10.1371/journal.pone.0151538. PubMed PMID: 26978272; PubMed Central PMCID: PMCPMC4792481.
30. Barry JM, Sakkaki S, Barriere SJ, Patterson KP, Lenck-Santini PP, Scott RC, et al. Temporal Coordination of Hippocampal Neurons Reflects Cognitive Outcome Post-febrile Status Epilepticus. EBioMedicine. 2016;7:175-90. doi: 10.1016/j.ebiom.2016.03.039. PubMed PMID: 27322471; PubMed Central PMCID: PMCPMC4909381.
31. Zutshi I, Brandon MP, Fu ML, Donegan ML, Leutgeb JK, Leutgeb S. Hippocampal Neural Circuits Respond to Optogenetic Pacing of Theta Frequencies by Generating Accelerated Oscillation Frequencies. Curr Biol. 2018;28(8):1179-88 e3. doi: 10.1016/j.cub.2018.02.061. PubMed PMID: 29628373.

32. Robinson J, Manseau F, Ducharme G, Amilhon B, Vigneault E, El Mestikawy S, et al. Optogenetic Activation of Septal Glutamatergic Neurons Drive Hippocampal Theta Rhythms. J Neurosci. 2016;36(10):3016-23. doi: 10.1523/JNEUROSCI.2141-15.2016. PubMed PMID: 26961955.
33. Laxpati NG, Mahmoudi B, Gutekunst CA, Newman JP, Zeller-Townson R, Gross RE. Real-time in vivo optogenetic neuromodulation and multielectrode electrophysiologic recording with NeuroRighter. Front Neuroeng. 2014;7:40. doi: 10.3389/fneng.2014.00040. PubMed PMID: 25404915; PubMed Central PMCID: PMCPMC4217045.
34. Blumberg BJ, Flynn SP, Barriere SJ, Mouchati PR, Scott RC, Holmes GL, et al. Efficacy of nonselective optogenetic control of the medial septum over hippocampal oscillations: the influence of speed and implications for cognitive enhancement. Physiol Rep. 2016;4(23). doi: 10.14814/phy2.13048. PubMed PMID: 27923975.
35. Shuman T, Amendolara B, Golshani P. Theta Rhythmopathy as a Cause of Cognitive Disability in TLE. Epilepsy Curr. 2017;17(2):107-11. doi: 10.5698/1535-7511.17.2.107. PubMed PMID: 28491003; PubMed Central PMCID: PMCPMC5416857.
36. Paxinos G, Watson C. The rat brain in stereotaxic coordinates. 4th ed. San Diego: Academic Press; 1998.
37. Kubie JL, Fenton A, Novikov N, Touretzky D, Muller RU. Changes in goal selection induced by cue conflicts are in register with predictions from changes in place cell field locations. Behavioral neuroscience. 2007;121(4):751-63. doi: 10.1037/0735-7044.121.4.751. PubMed PMID: 17663600.
38. Morris RG, Garrud P, Rawlins JN, O'Keefe J. Place navigation impaired in rats with hippocampal lesions. Nature. 1982;297(5868):681-3. PubMed PMID: 7088155.
39. Richard GR, Titiz A, Tyler A, Holmes GL, Scott RC, Lenck-Santini PP. Speed modulation of hippocampal theta frequency correlates with spatial memory performance. Hippocampus. 2013;23(12):1269-79. doi: 10.1002/hipo.22164. PubMed PMID: 23832676.
40. Wheeler. Methods for neural ensemble recordings. Boca Raton: CRC Press; 1999. 257 p. p.
41. Robbins AA, Fox SE, Holmes GL, Scott RC, Barry JM. Short duration waveforms recorded extracellularly from freely moving rats are representative of axonal activity. Front Neural Circuits. 2013;7:181. Epub 2013/12/19. doi: 10.3389/fncir.2013.00181. PubMed PMID: 24348338; PubMed Central PMCID: PMC3831546.
42. Fox SE, Ranck JB, Jr. Electrophysiological characteristics of hippocampal complex-spike cells and theta cells. Exp Brain Res. 1981;41(3-4):399-410. Epub 1981/01/01. PubMed PMID: 7215500.
43. Klausberger T, Somogyi P. Neuronal diversity and temporal dynamics: the unity of hippocampal circuit operations. Science. 2008;321(5885):53-7. doi: 10.1126/science.1149381. PubMed PMID: 18599766; PubMed Central PMCID: PMCPMC4487503.
44. Barry JM. Axonal activity in vivo: technical considerations and implications for the exploration of neural circuits in freely moving animals. Front Neurosci. 2015;9:153. doi: 10.3389/fnins.2015.00153. PubMed PMID: 25999806; PubMed Central PMCID: PMCPMC4422007.
45. Perkel DH, Gerstein GL, Moore GP. Neuronal spike trains and stochastic point processes. II. Simultaneous spike trains. Biophys J. 1967;7(4):419-40. doi: 10.1016/S0006-3495(67)86597-4. PubMed PMID: 4292792; PubMed Central PMCID: PMCPMC1368069.
46. Barry J, Muller R. Updating the hippocampal representation of space: place cell firing fields are controlled by a novel spatial stimulus. Hippocampus. 2011;21(5):481-94. Epub 2010/01/21. doi: 10.1002/hipo.20764. PubMed PMID: 20087890.

47. Fisher NI. Statistical analysis of circular data. Cambridge England ; New York, NY, USA: Cambridge University Press; 1993. xviii, 277 p. p.
48. Berens P. CircStat: A MATLAB Toolbox for Circular Statistics. J Stat Softw. 2009;31(10):1-21. PubMed PMID: WOS:000270513700001.
49. Ziegler A, Kastner C, Blettner M. The generalised estimating equations: An annotated bibliography. Biometrical J. 1998;40(2):115-39. doi: Doi 10.1002/(Sici)1521-4036(199806)40:2<115::Aid-Bimj115>3.0.Co;2-6. PubMed PMID: ISI:000074186100001.
50. Bender F, Gorbati M, Cadavieco MC, Denisova N, Gao X, Holman C, et al. Theta oscillations regulate the speed of locomotion via a hippocampus to lateral septum pathway. Nat Commun. 2015;6:8521. doi: 10.1038/ncomms9521. PubMed PMID: 26455912; PubMed Central PMCID: PMCPMC4633825.
51. Brandon MP, Koenig J, Leutgeb JK, Leutgeb S. New and Distinct Hippocampal Place Codes Are Generated in a New Environment during Septal Inactivation. Neuron. 2014;82(4):789-96. Epub 2014/05/24. doi: 10.1016/j.neuron.2014.04.013. PubMed PMID: 24853939.
52. Brandon MP, Bogaard AR, Libby CP, Connerney MA, Gupta K, Hasselmo ME. Reduction of theta rhythm dissociates grid cell spatial periodicity from directional tuning. Science. 2011;332(6029):595-9. Epub 2011/04/30. doi: 10.1126/science.1201652. PubMed PMID: 21527714; PubMed Central PMCID: PMC3252766.
53. Justus D, Dalugge D, Bothe S, Fuhrmann F, Hannes C, Kaneko H, et al. Glutamatergic synaptic integration of locomotion speed via septoentorhinal projections. Nat Neurosci. 2017;20(1):16-9. doi: 10.1038/nn.4447. PubMed PMID: 27893726.
54. McNaughton BL, Battaglia FP, Jensen O, Moser EI, Moser MB. Path integration and the neural basis of the 'cognitive map'. Nat Rev Neurosci. 2006;7(8):663-78. doi: 10.1038/nrn1932. PubMed PMID: 16858394.
55. Ketz N, Morkonda SG, O'Reilly RC. Theta coordinated error-driven learning in the hippocampus. PLoS Comput Biol. 2013;9(6):e1003067. doi: 10.1371/journal.pcbi.1003067. PubMed PMID: 23762019; PubMed Central PMCID: PMCPMC3675133.
56. Leao RN, Mikulovic S, Leao KE, Munguba H, Gezelius H, Enjin A, et al. OLM interneurons differentially modulate CA3 and entorhinal inputs to hippocampal CA1 neurons. Nat Neurosci. 2012;15(11):1524-30. doi: 10.1038/nn.3235. PubMed PMID: 23042082; PubMed Central PMCID: PMCPMC3483451.
57. Petsche H, Gogolak G, Stumpf C, Newkirk T. [the Alteration of Theta Rhythm in the Rabbit Hippocampus by Electrical Stimulation of the Septum and Reticular Formation]. Pflugers Arch Gesamte Physiol Menschen Tiere. 1964;278:520-31. PubMed PMID: 14126447.
58. Simon AP, Poindessous-Jazat F, Dutar P, Epelbaum J, Bassant MH. Firing properties of anatomically identified neurons in the medial septum of anesthetized and unanesthetized restrained rats. J Neurosci. 2006;26(35):9038-46. doi: 10.1523/JNEUROSCI.1401-06.2006. PubMed PMID: 16943562.
59. Zhang H, Lin SC, Nicolelis MA. Spatiotemporal coupling between hippocampal acetylcholine release and theta oscillations in vivo. J Neurosci. 2010;30(40):13431-40. doi: 10.1523/JNEUROSCI.1144-10.2010. PubMed PMID: 20926669; PubMed Central PMCID: PMCPMC2988451.
60. Vandecasteele M, Varga V, Berenyi A, Papp E, Bartho P, Venance L, et al. Optogenetic activation of septal cholinergic neurons suppresses sharp wave ripples and enhances theta oscillations in the hippocampus. Proc Natl Acad Sci U S A. 2014;111(37):13535-40. doi: 10.1073/pnas.1411233111. PubMed PMID: 25197052; PubMed Central PMCID: PMCPMC4169920.

61. Koenig J, Linder AN, Leutgeb JK, Leutgeb S. The spatial periodicity of grid cells is not sustained during reduced theta oscillations. Science. 2011;332(6029):592-5. doi: 10.1126/science.1201685. PubMed PMID: 21527713.
62. Schomburg EW, Fernandez-Ruiz A, Mizuseki K, Berenyi A, Anastassiou CA, Koch C, et al. Theta phase segregation of input-specific gamma patterns in entorhinal-hippocampal networks. Neuron. 2014;84(2):470-85. doi: 10.1016/j.neuron.2014.08.051. PubMed PMID: 25263753; PubMed Central PMCID: PMC4253689.
63. Wang Y, Romani S, Lustig B, Leonardo A, Pastalkova E. Theta sequences are essential for internally generated hippocampal firing fields. Nat Neurosci. 2015;18(2):282-8. doi: 10.1038/nn.3904. PubMed PMID: 25531571.
64. Lipponen A, Woldemichael BT, Gurevicius K, Tanila H. Artificial theta stimulation impairs encoding of contextual fear memory. PLoS One. 2012;7(11):e48506. doi: 10.1371/journal.pone.0048506. PubMed PMID: 23133638; PubMed Central PMCID: PMCPMC3486864.
65. McNaughton N, Ruan M, Woodnorth MA. Restoring theta-like rhythmicity in rats restores initial learning in the Morris water maze. Hippocampus. 2006;16(12):1102-10. doi: 10.1002/hipo.20235. PubMed PMID: 17068783.
66. Shirvalkar PR, Rapp PR, Shapiro ML. Bidirectional changes to hippocampal theta-gamma comodulation predict memory for recent spatial episodes. Proc Natl Acad Sci U S A. 2010;107(15):7054-9. doi: 10.1073/pnas.0911184107. PubMed PMID: 20351262; PubMed Central PMCID: PMCPMC2872428.
67. Turnbull J, Jiang F, Racine R. Hippocampal stimulation of fornical-lesioned rats improves working memory. Can J Neurol Sci. 1994;21(2):100-3. PubMed PMID: 8087733.
68. Lee DJ, Izadi A, Melnik M, Seidl S, Echeverri A, Shahlaie K, et al. Stimulation of the medial septum improves performance in spatial learning following pilocarpine-induced status epilepticus. Epilepsy Res. 2017;130:53-63. doi: 10.1016/j.eplepsyres.2017.01.005. PubMed PMID: 28152425.
69. Winson J. Loss of hippocampal theta rhythm results in spatial memory deficit in the rat. Science. 1978;201(4351):160-3. PubMed PMID: 663646.
70. Geisler C, Robbe D, Zugaro M, Sirota A, Buzsaki G. Hippocampal place cell assemblies are speed-controlled oscillators. Proc Natl Acad Sci U S A. 2007;104(19):8149-54. doi: 10.1073/pnas.0610121104. PubMed PMID: 17470808; PubMed Central PMCID: PMCPMC1876586.
71. Krakauer JW, Ghazanfar AA, Gomez-Marin A, MacIver MA, Poeppel D. Neuroscience Needs Behavior: Correcting a Reductionist Bias. Neuron. 2017;93(3):480-90. doi: 10.1016/j.neuron.2016.12.041. PubMed PMID: 28182904.
72. Ezzyat Y, Kragel JE, Burke JF, Levy DF, Lyalenko A, Wanda P, et al. Direct Brain Stimulation Modulates Encoding States and Memory Performance in Humans. Curr Biol. 2017;27(9):1251-8. doi: 10.1016/j.cub.2017.03.028. PubMed PMID: 28434860.
73. Jacobs J, Miller J, Lee SA, Coffey T, Watrous AJ, Sperling MR, et al. Direct Electrical Stimulation of the Human Entorhinal Region and Hippocampus Impairs Memory. Neuron. 2016;92(5):983-90. doi: 10.1016/j.neuron.2016.10.062. PubMed PMID: 27930911.
74. Coleshill SG, Binnie CD, Morris RG, Alarcon G, van Emde Boas W, Velis DN, et al. Material-specific recognition memory deficits elicited by unilateral hippocampal electrical stimulation. J Neurosci. 2004;24(7):1612-6. doi: 10.1523/JNEUROSCI.4352-03.2004. PubMed PMID: 14973245.

Figure Legends

Figure 1: Immunohistochemistry and experimental approach. A) Top Left - Example of MS CHR2 expression using EYFP light microscopy. Bottom Left -Hippocampal GAD expression (white arrows) in red reveals OLM interneurons in str. Oriens and basket cells in str. Pyramidale that synapse with virally transfected MS axons (EYFP). DAPI stained cell nuclei are visible in blue. Top Right - MS GAD stained GABAergic cell bodies in red co-localized with GFP and DAPI (white arrows). Middle Right - MS Chat stained cholinergic cell bodies in red co-localized with GFP and DAPI (white arrows). Bottom right – MS VGLUT stained glutamatergic cell bodies in red co-localized with GFP and DAPI (white arrows). The AAV therefore transfects both cholinergic and GABAergic cells in the MS whose axonal projections can be traced to hippocampal interneurons, illustrating the circuit and microcircuit levels by which MS stimulation paces hippocampal theta. B) Experimental approach using optogenetics and electrophysiology in the dorsal hippocampus and MS via custom devices for the delivery of an optical fiber and EEG electrodes in the MS and tetrode array in the hippocampus. C) Protocol for experiment 1 where electrophysiological recordings occurred during 6 min of 6 Hz MS stimulations at both control Y and experimental B stimulation while the rat rests at the bottom of a tall, narrow flowerpot. D) Protocol for experiment 2 where electrophysiological recordings are carried out during 30 min of 6 Hz MS stimulations at both Y and B wavelengths while the rat performs a spatial accuracy task that is hippocampus-independent (Cued: Top), and a spatial accuracy task that is hippocampus-dependent (Uncued: Bottom).

Figure 2: Six min of 6 Hz Y and B MS stimulation and recording in a narrow flowerpot. A) Representative results from approximately 20 sec epochs of raw EEG and corresponding spectrogram of CA1 (Top) and MS (Bottom) signals during Y (Left) and B stimulation (Right). Theta band signals are indicated by black arrows. B) Amplitude for 6 min Y and B stimulation epochs in hippocampus (Top) and MS (Bottom) suggests peak amplitude shifts to 6 Hz, matching the MS input frequency. C) Mean normalized firing probability of simultaneously recorded cells in str. pyramidale, 17 pyramidal cells (PYR in red) and 6 putative basket cells (BaC in green), and 3 putative OLM cells from str. oriens (black) during Y (Top) and B (Bottom) MS stimulation relative to local theta from each hippocampal layer (Left) and MS theta (Right). Firing phase of hippocampal cells is significantly reorganized relative to local and septal theta references. B stimulation causes peak pyramidal cell activity to occur between the peaks of both interneuron types. In comparison to local theta reference, which represents multiple theta inputs, hippocampal cell activity referenced to MS theta suggests the MS exerts temporal control over the interneurons as denoted by distinct firing probability peaks and valleys in response to B stimulation. D) Example rose plot histograms for each MS referenced neuron type in C during Y (Top) and B (Bottom) MS stimulation. The resultant theta phase vector (RBAR) and significance (p-value) for each cell is shown. As indicated by firing probability plots in C, interneurons become phase locked to the artificial MS signal. BC and OLM are phase locked to opposite phases of MS theta and PYR cells fire between these phases. Temporal organization of PYR cells is therefore sculpted by putative OLM and basket cell interneuron types which are, in turn, heavily influenced by the artificial MS signal.

Figure 3: Mean and SE of normalized theta amplitude, peak theta amplitude and peak theta frequency in the hippocampus (A) and MS (B) during 6 Hz Y and B stimulation. Dashed black lines indicate data from individual animals. C) Phase preference circular statistics for hippocampal CA1 pyramidal cells from all 3 animals (n= 64) during 6 Hz Y (Left) and B (Right) MS stimulation epochs relative to local hippocampal theta (Top) and MS theta (Bottom). Each circle represents the mean angle and magnitude of phase preference for an individual pyramidal cell. The arrow indicates the mean angle and significance of the resultant population phase

vector. RBAR levels for the circular plot are shown in red and mean vector RBAR is presented at the tip of each arrow. A red asterisk denotes significance. During Y stimulation (Left), the hippocampal cell population has a robust mean resultant vector (Arrow) at 66° relative to local theta and a weaker resultant vector at 0° relative to septal theta. During B MS stimulation, the cell phase vectors relative to both references shift into alignment toward the trough of theta (Right). The significance and magnitude of the phase preference (p and RBAR values) as well as the mean direction (MeanDir) are shown. D) Septal stimulation does not change the mean RBAR of each cell relative to local theta but does cause a significant increase relative to the septal signal. E-F) Example autocorrelation histograms (HAC) during 6 Hz Y (Left) and B (Right) stimulation for example interneurons (E) and pyramidal cells (F) from the same dataset in C. B stimulation clearly biases the spike timing of a subset of pyramidal neurons toward intervals that match the 6 Hz MS input frequency.

Figure 4: Examples of hippocampus and MS speed/theta dynamics relative to stimulation (Y vs. B) and spatial accuracy (Cued vs. Uncued) conditions. A) Mean theta amplitude by frequency during slow (blue lines) and fast (black lines) velocities (*v*) during Y MS stimulation in the cued spatial accuracy task (Top Left). The relationship between movement speed and the frequency of each theta cycle (blue dots) is illustrated beneath the amplitude by frequency plot for each condition. The line of best fit (black line) and the corresponding correlation coefficient between theta frequency and speed indicate a significantly linear relationship (r and p values indicated above plot). Plots from both Y and B stimulations for cued and uncued conditions are presented relative to local theta (A) and MS theta (B). In the cued session, mean theta peaks occur at the MS input frequency at 6 Hz when the rat is moving less than 2 cm/s. At faster speeds, theta toggles to a higher frequency that still increases linearly with speed. In contrast, this endogenous compensatory theta signal is absent in the uncued session during B MS stimulation and theta oscillates at the MS input frequency at 6 Hz. B) As in A, plots for examples of simultaneously recorded MS theta signals. During Y stimulation speed/theta correlation is less robust in the MS, although there is a marked increase in r during the uncued session. During B MS stimulation, theta signals are fixed at the 6 Hz input frequency regardless of speed. C) Peak hippocampal theta frequency and amplitude during speeds ≥ 5 cm/s (Left) and ≤ 2cm/s (Middle) as well as mean theta frequency and normal mean theta amplitude at movement speeds (Right) during 6 Hz Y stimulation in the cued (YC) and uncued session (YUC) and during 6 Hz B stimulation in the cued (BC) and uncued (BUC) session. Compared to YC and YUC, mean peak theta frequency across animals significantly increases in the BC session and significantly decreases in the BUC session. This corresponds to the presence and absence of the compensatory intrinsic theta oscillations in each session. As overall mean frequency was not significantly different between BC and either YC or YUC sessions, this further implies that the peak frequency shift in BC is caused by a drive to maintain mean theta frequency in this condition. This drive toward the mean was not found during BUC. While theta amplitude was significantly decreased relative to baseline during BC and BUC during fast speeds, there were no significant changes by task condition during slow speeds or in mean normalized theta amplitude. D) As in C for speed and theta property dynamics by task condition for MS signals. There are no significant peak theta differences relative to baseline in either BC and BUC, yet peak frequency is unanimously at 6 Hz for all 3 animals at both speed ranges. Mean frequency is also at 6 Hz during BC and BUC. Peak theta amplitude and mean theta amplitude increase significantly relative to baseline at both speed ranges. E) Mean correlation between speed and hippocampal (Left) and MS (Right) theta frequency for all rats. Speed/theta r value increases significantly relative to YC during YUC and remains high during BC. Speed/theta r value decreases significantly during BUC due to the absence of compensatory intrinsic theta. The speed and MS theta frequency relationship is abolished in both BC and BUC task conditions.

Figure 5: Example theta phase preference circular statistics for CA1 pyramidal cells (n=57) relative to both local hippocampal theta and MS theta from 1 animal during 6 Hz Y and B stimulation (Top and Bottom of each section respectively) in the cued (YC and BC in A) and uncued (YUC and BUC in B) spatial accuracy tasks. Each circle represents the mean angle and magnitude of resultant theta phase vector (RBAR) for an individual pyramidal cell. The arrow indicates the mean angle and magnitude of resultant theta phase vector for the population. Discontinuous arrowheads indicate resultant vectors > 0.2. RBAR levels for the circular plot are shown in red. The p-values, population RBAR values and mean phase vector angle (MeanDir) are shown above each plot in A-B. Significant (red asterisks) and non-significant vectors (ns) are noted. A) During YC, cells have a significant phase preference relative to local hippocampal theta and septal theta that are approximately 180° apart. During BC, the cells have no significant phase preference relative to local theta while the phase vector relative to septal theta remains significant, although shifted 126° from baseline. B) As in A, during BUC the mean resultant length of the hippocampal theta phase vector is no longer significant. The mean septal theta phase vector remains significant but shifts 152° relative to baseline. During BUC, the septal theta phase vector occupies a similar phase space as baseline hippocampal theta during YUC. This may reflect competing inputs over CA1 cell activity during B MS stimulation at peak theta phase. C-D) Mean and standard error of the population vector RBAR (Left) and population dispersion (Right) for all 3 rats relative to hippocampal theta (C) and septal theta (D). During BUC, the mean population vector relative to hippocampal theta had the lowest population RBAR and the highest levels of dispersion. Both variables during BUC were significantly different from YC and YUC. No significant effects of stimulation/task condition were found relative to septal theta. E) Relative to septal theta, the difference of the mean population vector during YUC and BUC (MSYUC-MSBUC in grey column) was greater than the difference of the mean vector between YC and BC (MSYC-MSBC in black column), indicating task differences in the phase separation of septal inputs during B stimulation. F) The difference between the mean hippocampal and septal phase vector during YUC (HCYUC-MSYUC in yellow column) is typically ~180°, indicating that the phase vectors of local and septal inputs tend to be at opposite phases during the uncued task. The mean difference between the septal vector during BUC and the baseline hippocampal vector during YUC (HCYUC-MSBUC in black column) is significantly reduced. This reiterates the observation in E that the 180° shift in septal phase preference puts the septal vector during BUC and the hippocampal vector during baseline in YUC in the same phase space. This phenomenon may represent the competition of local and septal inputs over the coordination of CA1 cell activity and the superseding of local theta by MS theta during B stimulation.

Figure 6: Stimulation and task conditional effects on the timing of CA1 pyramidal neuron inter-spike intervals. A) Example autocorrelation histograms (Left) and autocorrelograms (Right) for a pyramidal cell during 6 Hz Y MS stimulation in the cued (YC) and uncued (YUC) tasks and during 6 Hz B MS stimulation during the cued (BC) and uncued (BUC) tasks. Frequency (FR), modulation depth (MD), and peak autocorrelation (right of each peak) are shown in each condition. The periodicity and modulation depth of the example cell during BUC indicate prominent changes in modulation depth and periodicity indicating entrainment at the septal input frequency of 6 Hz. Periodicity and modulation depth for the cell are constant during both baseline conditions while the cell is poorly modulated during BC. B) Mean and standard error of inter-spike interval modulation depth across animals during each stimulation and task condition. Mean modulation depth decreases significantly during B stimulations conditions, and significantly lower than all other conditions during BUC. However, as shown in the inset, analysis of variance for the modulation depth of all cells that were < or ≥ 9 Hz reveals a separation of frequency entrainment by condition. Approximately 70% of all cells exhibit beat frequency ≥ 9 Hz and are significantly less modulated in both BC and BUC and are negligibly modulated during BUC. C) Mean and standard error of modulation frequency as estimated through inter-spike interval periodicity across animals during each stimulation and task condition. As beat frequency may be

overestimated when the cell is poorly modulated, modulation depth is used as a covariate in general estimating equation analysis. In both Y baseline conditions and BC, the mean frequency is approximately 9Hz but decreases significantly during BUC. D) Histogram representing the number of cells by modulation frequency in each task and stimulation condition with overlaid normality distribution curves. The dashed line serves as a reference point for the mean LFP theta frequency during YC, YUC and BC at 7.5 Hz. The majority of cells during baseline conditions are clustered ~ 1 Hz ahead of the mean theta frequency. While task condition has little effect on the distribution of cell periodicity during YC and YUC, during BC the distribution shifts to higher frequencies and has a peak at 9 Hz. During BUC the distribution appears bimodal with 2 populations separated at approximately 7.5 Hz and a peak at 11 Hz. E) As modulation frequency can be overestimated with low modulation, the frequency data from D are presented in a scatterplot against modulation depth for each condition. Each circle represents data from a single pyramidal cell and the dashed line again serves as a reference for mean LFP theta during YC, YUC and BC at 7.5 Hz. A separation of cells into 2 populations exhibiting modulation frequencies either > or < 7.5 Hz is now evident during BC. As suggested by the inset in B, during BC 30% of the cells shift toward the input frequency at 6 Hz while the remainder of well modulated cells shift toward faster frequencies or exhibit attenuated modulation. During BUC, the subset of cells < 7.5 Hz are still well modulated while those > 7.5 Hz are not. Spike timing results therefore reiterate the bisection of local theta oscillations between septal input frequency and a compensatory endogenous theta frequency during BC, as well as the attenuation of endogenous theta influence during BUC.

Figure 7: Examples of simultaneously recorded place cell firing fields during each task and stimulation condition (A) and the results of field property analysis between conditions (B). Although LFP, phase preference and the temporal organization of spike timing are significantly altered by B stimulation, task and stimulation conditions did not cause significant changes to mean field coherence, mean overall rate, mean firing field stability, mean firing field size, mean in-field firing rate or mean out-field firing rate. Although temporal coordination is altered, spatial coding remains the same. This allows us to ask whether intrinsic theta oscillations are necessary

Figure 8: A-C) Three examples of spatial accuracy behavior are shown during each task and stimulation condition. Each subsection consists of a speed map (cm/s) and dwell time map (% of overall time) that generally have an inverse relationship as the rats cumulatively spend the majority of the session time paused in the goal zone. Black circles in the speed maps indicate the diameter of the rat's mean search accuracy in the target quadrant. Cued sessions are on the top row while uncued sessions are on the bottom row. Y stimulation sessions are at left and B stimulation sessions are at right. Relative to baseline performance during YC, B stimulation during BC had no effect on the rat's ability to find the goal zone. In contrast, B stimulation during BUC (Dashed outline) generally caused the rat to broaden its search for the goal zone throughout the target quadrant (A and B) or to consistently search in the same off target location (C). D) Mean and standard error of the behavioral properties of spatial accuracy across animals with 3-4 repeated series of each stimulus and task condition per animal. The mean number of rewards (Top) across rats was significantly greater in the cued than uncued sessions, inferring that the uncued task was more difficult than the cued task. In addition, the mean search pattern tended to be closer to the goal center in the x-axis (Middle) and the y-axis (Bottom) during the cued rather than uncued sessions. The rats received the fewest rewards during BUC and significantly fewer rewards during BUC than during the baseline performance in YUC. Significant differences were found between the mean search pattern accuracy in the y-axis during YUC and BUC. This suggests that the further the rats were from the arena wall in the target quadrant during BUC, the more likely they were to search an average of 5.24 pixels (~ 2 cm) further away from the goal than during YUC.

Supplemental Figure 1: A) Example spike timing measurements for modulation frequency and modulation depth of a hippocampal interneuron during 6 Hz Y (Top) and B (Bottom) MS stimulation. For both conditions autocorrelation histograms (HAC at Left) and autocorrelograms (ACG at Right) are shown. Peak autocorrelation values are shown to the right of the peak ACG. The + symbols indicate the algorithm's search for autocorrelation peaks in order to calculate periodicity while the green circles indicate the algorithm's measurement of modulation depth between peaks and valleys. Modulation frequencies tend to be high (i.e. > 9 Hz) when the modulation depth is low (i.e. < 0.001). B) Table illustrating the mean overall rate, modulation frequency and modulation depth of the example interneuron in A. While the cell's firing rate remains constant, its modulation frequency and modulation depth are markedly altered to match the 6 Hz MS input signal during B stimulation.

Supplemental Figure 2: Histology of optical and recording probe sites in the MS (A) and the dorsal hippocampus (B). A) Virally transfected MS axons and neurons in green (EYFP), DAPI stained cell nuclei are visible in blue while GABAergic neurons are indicated in red (GAD). Dark areas indicate tracks occupied by the optical probe and EEG wires (Top) and the initial viral injection via the Hamilton syringe (Bottom). These regions are in the center of the MS, flanked by the ventral region of the lateral septum nucleus and the anterior commissure, above the horizontal and vertical limbs of the diagonal band of Broca (hDB and vDB). B) Recording tetrode tracks through the neocortex and CA1 of the dorsal hippocampus (White Arrows). Note heavy projection of transfected MS axons to the alveus layer and the dentate gyrus.

Supplemental Figure 3: Full 6 min spectrogram data from the example shown in Figure 3 for both hippocampus (Top) and MS (Bottom) during Y (A) and B (B) stimulation s. Color continuum at right indicates signal amplitude (A.U.).

Supplemental Figure 4: Scatter plot of MS peak theta amplitude (y-axis) by peak theta frequency (x-axis) during 6 Hz Y (yellow dots) and B (blue dots) stimulation epochs per animal in experiment 1. The dashed black line shows the mean frequency and amplitude for all 3 subjects.

Supplemental Figure 5: Spike timing population dynamics during 6 Hz Y and B MS stimulation. A) Histograms illustrating spike timing alterations for a subset of neurons with a resultant modulation depth > 0.01 during B stimulation. B-C) Scatter plots of modulation depth against mean overall rate (Left B) and modulation frequency (Left C). The modulation depth during B stimulation was then ranked and the population split between the top 25% of the most modulated cells (U25MD) and plotted against mean overall rate (middle B) and modulation frequency (middle C) for each stimulation condition. This was then repeated for the remaining 75% of the cell population (R75MD) and shown at the right of B and C. D) Mean and standard error for the overall rate, modulation frequency and modulation depth of each cell population (U25MD vs. R75MD) during each stimulation condition. While mean overall rate does not change during B stimulation for either population, U25MD cells tend to have a higher mean baseline-firing rate (Left). These cells are also more likely to shift frequency to match the MS input frequency at 6 Hz (Middle). As the defining feature of this subpopulation, their modulation depth increases significantly during B MS stimulation (Right).

Supplemental Figure 6: Speed sorted spectrograms (Top of each plot) and animal speed (Bottom each plot) for CA1 theta oscillations during 6 Hz Y stimulation in the cued (Top Left), and uncued (Bottom Left) spatial accuracy task. Theta amplitude (Color bar at right in A.U.) and frequency increase linearly with speed. Black arrowheads indicate epochs of the speed sorted spectrograms that have been expanded beneath each plot. B) As in A for 6 Hz B stimulation in the cued (Top Right) and uncued (Bottom right) spatial accuracy task. During B stimulation in the cued task, theta frequency toggles between the input frequency and approximately 9 Hz. During B

stimulation during the uncued version of the task, theta frequency predominately oscillates at the MS input frequency at 6 Hz.

Supplemental Figure 7: Sample LFP and spike timing results during B MS stimulation at 10 Hz. A) Speed/theta relationship as in supplemental figure 6. Stimulation during performance of the cued task causes an inversion of the speed/theta relationship. At slow movement speeds the majority of the theta band signal oscillates at 10 Hz. As the animal moves faster the theta signal shifts toward slower frequencies < 8 Hz, resulting in a significantly negative speed/theta relationship (Right). B) Similar to the result found for 6 Hz stimulation, 10 Hz MS stimulation during the uncued version of the task results in theta band oscillations that more faithfully mirror the MS input frequency regardless of movement speed. C) Autocorrelation histograms (inset) and autocorrelograms illustrating theta modulation through inter-spike interval lag times for a CA1 pyramidal cell in each version of the spatial accuracy task during 10 Hz Y and B stimulation. Peak autocorrelation, frequency (FR) and modulation depth (MD) are shown. As determined by frequency, the example cell is heavily modulated at 8.3 Hz during both the cued and uncued versions of the task. While the cell loses modulation during 10 Hz B stimulation in the cued task, it is robustly modulated at the septal input frequency during the uncued version of the task.

Supplemental Table 1: Mean + SE for speed and CA1 speed/theta properties by task condition across all 3 animals during 10 Hz B stimulation.

Supplemental Figure 8: Examples of CA1 speed/theta properties from one animal during 2 consecutive food pellet foraging sessions (A-B) where theta frequency reliably increases with movement speed in the absence of cognitive demand.

Supplemental Table 2: Mean + SE for speed and CA1 speed/theta properties in each of the 2 foraging sessions across 3 animals. Peak theta frequency is faster during speeds ≥ 5 cm/s than speeds ≤ 2 cm/s. Mean speed/theta correlation in this context is on par with the cued version of the spatial accuracy task during Y stimulation.

Supplemental Figure 9: A-B) From the same examples shown in Fig. 5, comparisons of firing probability mean + SE for all cells by local (Top) and septal (Bottom) theta phase (30° bins) in each task/stimulation condition. Yellow lines indicate 6 Hz Y MS stimulation while blue lines indicate 6 Hz B MS stimulation. Hippocampal theta phase preference is abolished in both BC and BUC as indicated by the relatively flat lines in both conditions. The more pronounced phase preference peak and valley during YUC are particularly evident in comparison with BUC. With regard to the septal theta reference, B stimulation shifted peak phase preference approximately 180° in both task conditions, aligning peak hippocampal theta phase preferences with yellow stimulation in baseline conditions (black arrows). C) Firing probability mean + SE for all CA1 pyramidal cells recorded from 3 animals (n=158) while foraging for food pellets. Firing probability distribution and peak is similar to the YC condition in A. D) Pooled hippocampal theta phase preference circular statistics for cells in D. Each black circle represents the mean angle and magnitude of resultant theta phase vector (RBAR) for an individual pyramidal cell. The arrow indicates the mean angle and magnitude of phase preference for the resultant population phase vector. RBAR levels for the circular plot are shown in red. The p-values, population RBAR values and mean phase vector angle (MeanDir) are shown above the plot. The phase preference is diffuse across animals yet has a significant mean phase vector at a similar angle as the example during YC. This suggests a continuum of phase preference in relation to cognitive demand between foraging, the cued spatial task and the uncued spatial task.

Supplemental Figure 10: Examples of spatial accuracy behavior as in Figure 9 A and C, featuring path (Grey lines), mean search pattern diameter (Black dashed circle) and the center of mean search accuracy (Red circle) relative to the goal zone (Blue circle). A red line represents radius angle from the apparatus center to the arena periphery through the center of the search pattern.

In A, B stimulation causes the rat to broaden the search for the goal zone while in B it causes the rat to consistently search for the goal in an incorrect location.

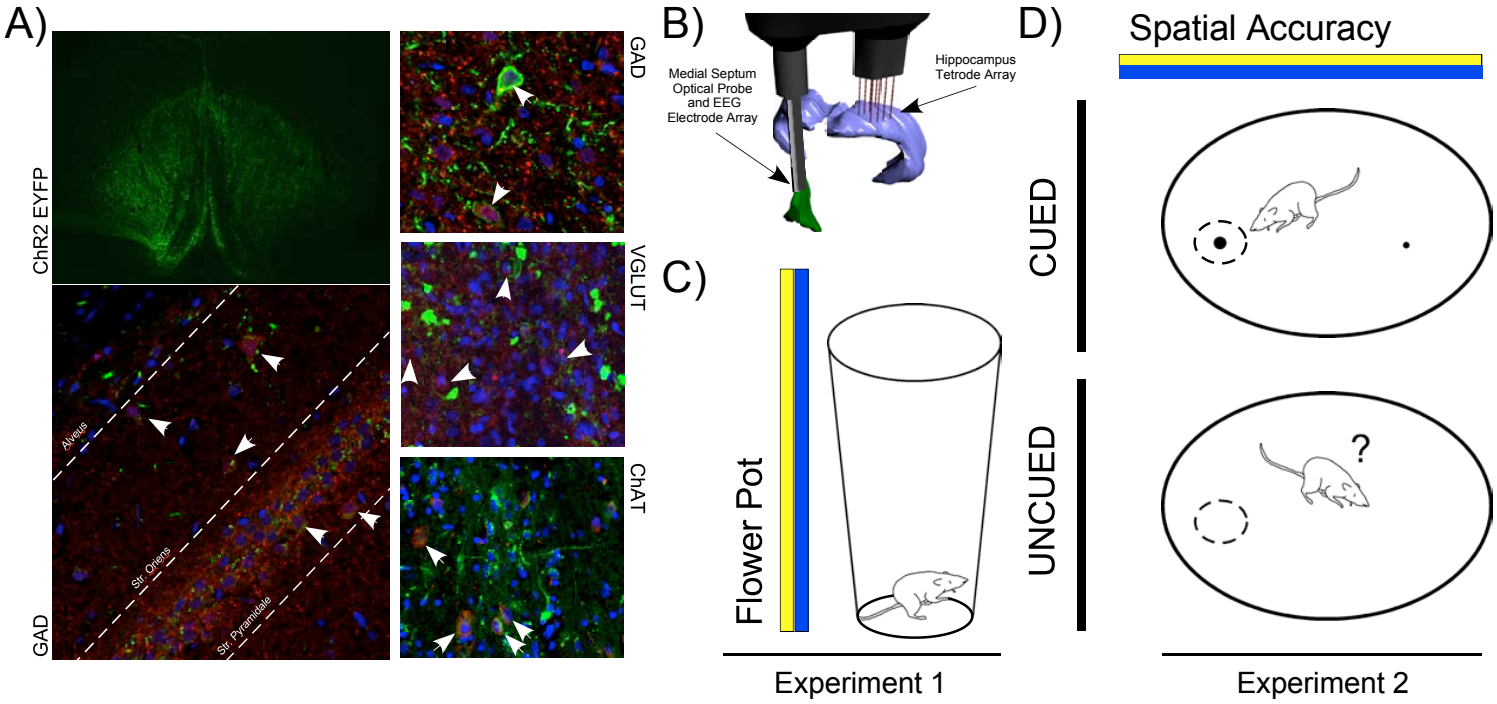
A)
ChR2 EYFP
GAD
GAD
VGLUT
ChAT
Alveus
Str. Oriens
Str. Pyramidale
B)
Medial Septum
Optical Probe
and EEG
Electrode Array
Hippocampus
Tetrode Array
C)
Flower Pot
Experiment 1
D)
Spatial Accuracy
CUED
UNCUED
?
Experiment 2

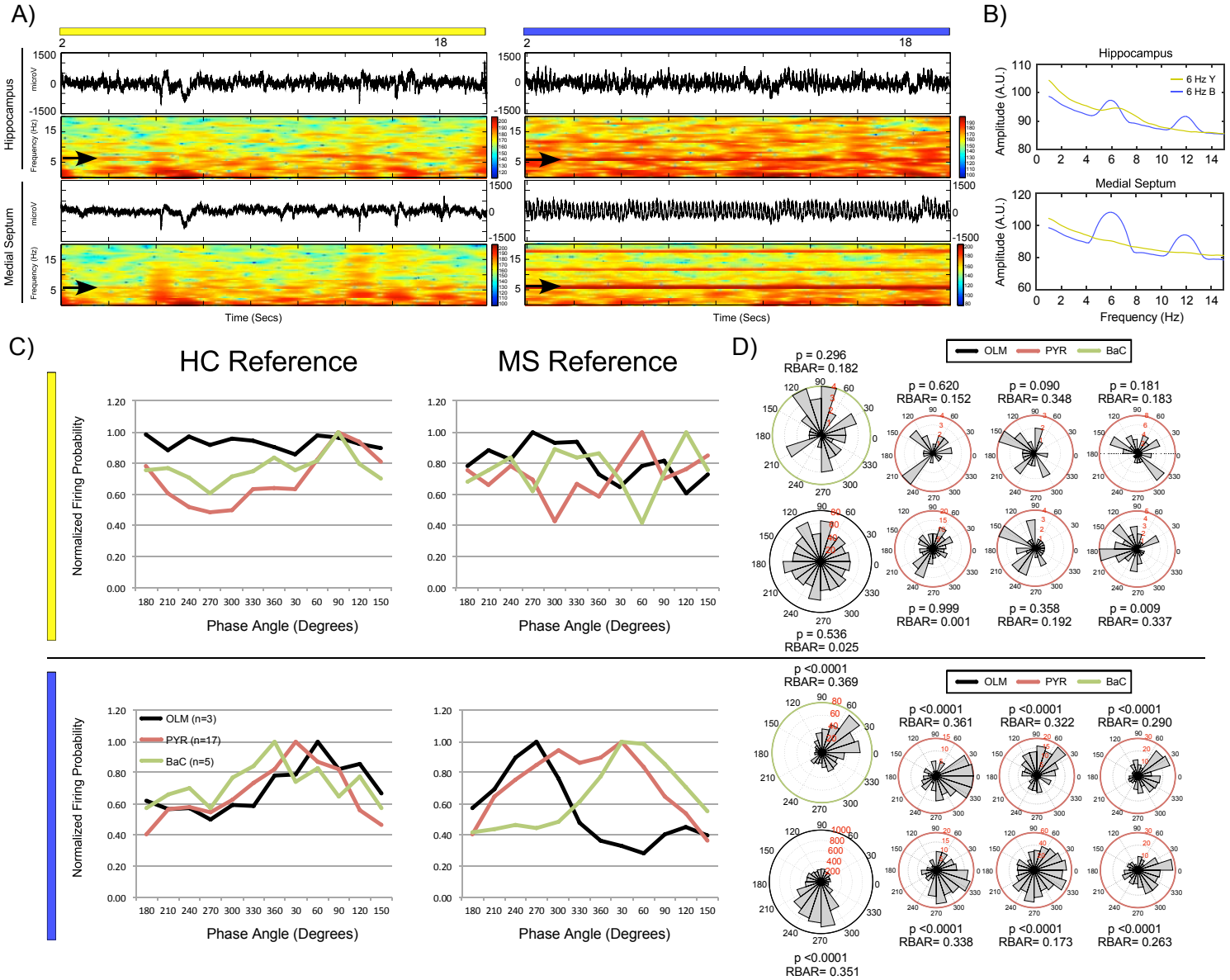
A)
Hippocampus
Medial Septum
microV
Frequency (Hz)
Time (Secs)
B)
Hippocampus
6 Hz Y
6 Hz B
Amplitude (A.U.)
Medial Septum
Frequency (Hz)
C)
HC Reference
MS Reference
Normalized Firing Probability
Phase Angle (Degrees)
OLM (n=3)
PYR (n=17)
BaC (n=5)
D)
OLM
PYR
BaC
p = 0.296
RBAR= 0.182
p = 0.620
RBAR= 0.152
p = 0.090
RBAR= 0.348
p = 0.181
RBAR= 0.183
p = 0.536
RBAR= 0.025
p = 0.999
RBAR= 0.001
p = 0.358
RBAR= 0.192
p = 0.009
RBAR= 0.337
p <0.0001
RBAR= 0.369
p <0.0001
RBAR= 0.361
p <0.0001
RBAR= 0.322
p <0.0001
RBAR= 0.290
p <0.0001
RBAR= 0.351
p <0.0001
RBAR= 0.338
p <0.0001
RBAR= 0.173
p <0.0001
RBAR= 0.263

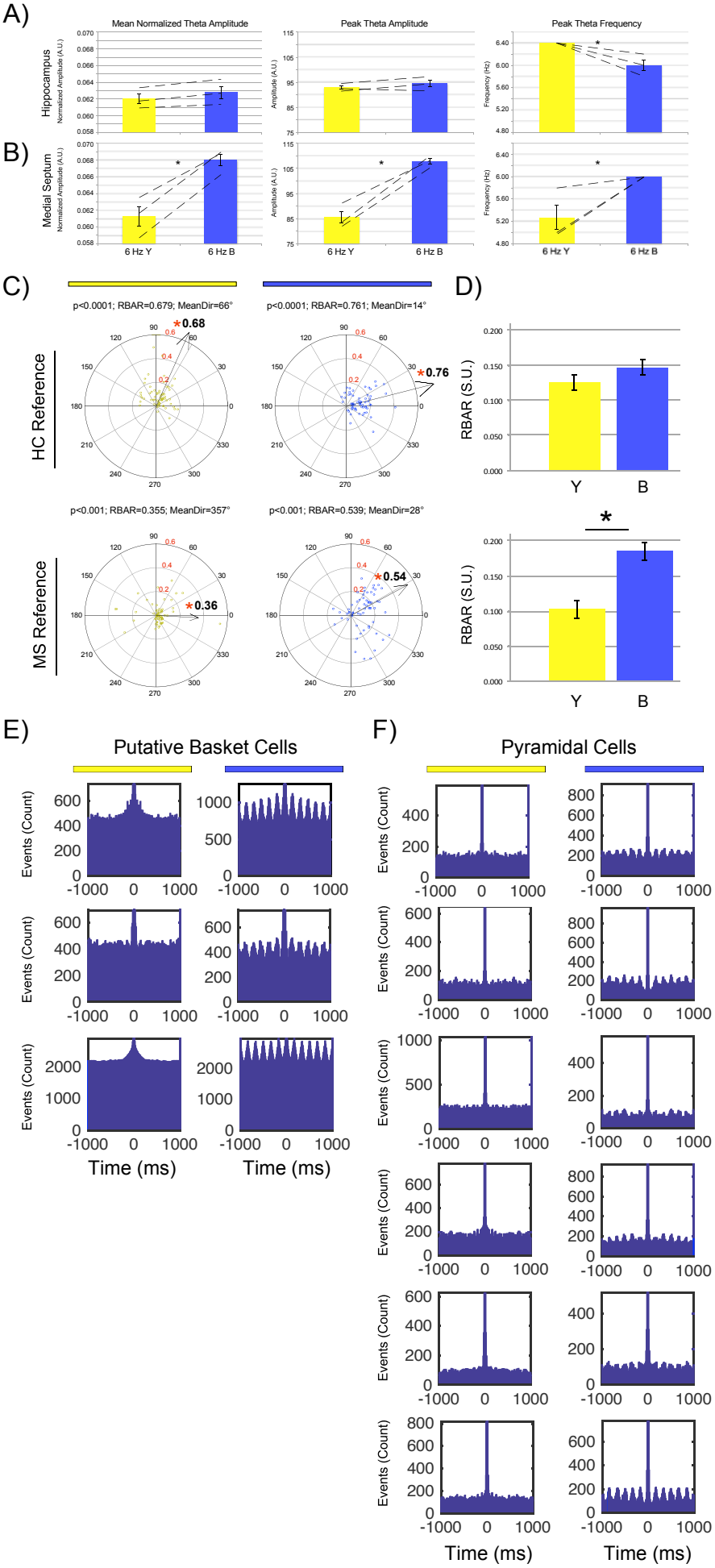
A)
Mean Normalized Theta Amplitude
Peak Theta Amplitude
Peak Theta Frequency
Hippocampus
Normalized Amplitude (A.U.)
Amplitude (A.U.)
Frequency (Hz)
B)
Medial Septum
6 Hz Y
6 Hz B
C)
p<0.0001; RBAR=0.679; MeanDir=66°
p<0.0001; RBAR=0.761; MeanDir=14°
0.68
0.76
HC Reference
p<0.001; RBAR=0.355; MeanDir=357°
p<0.001; RBAR=0.539; MeanDir=28°
0.36
0.54
MS Reference
D)
RBAR (S.U.)
Y
B
E)
Putative Basket Cells
Events (Count)
Time (ms)
F)
Pyramidal Cells

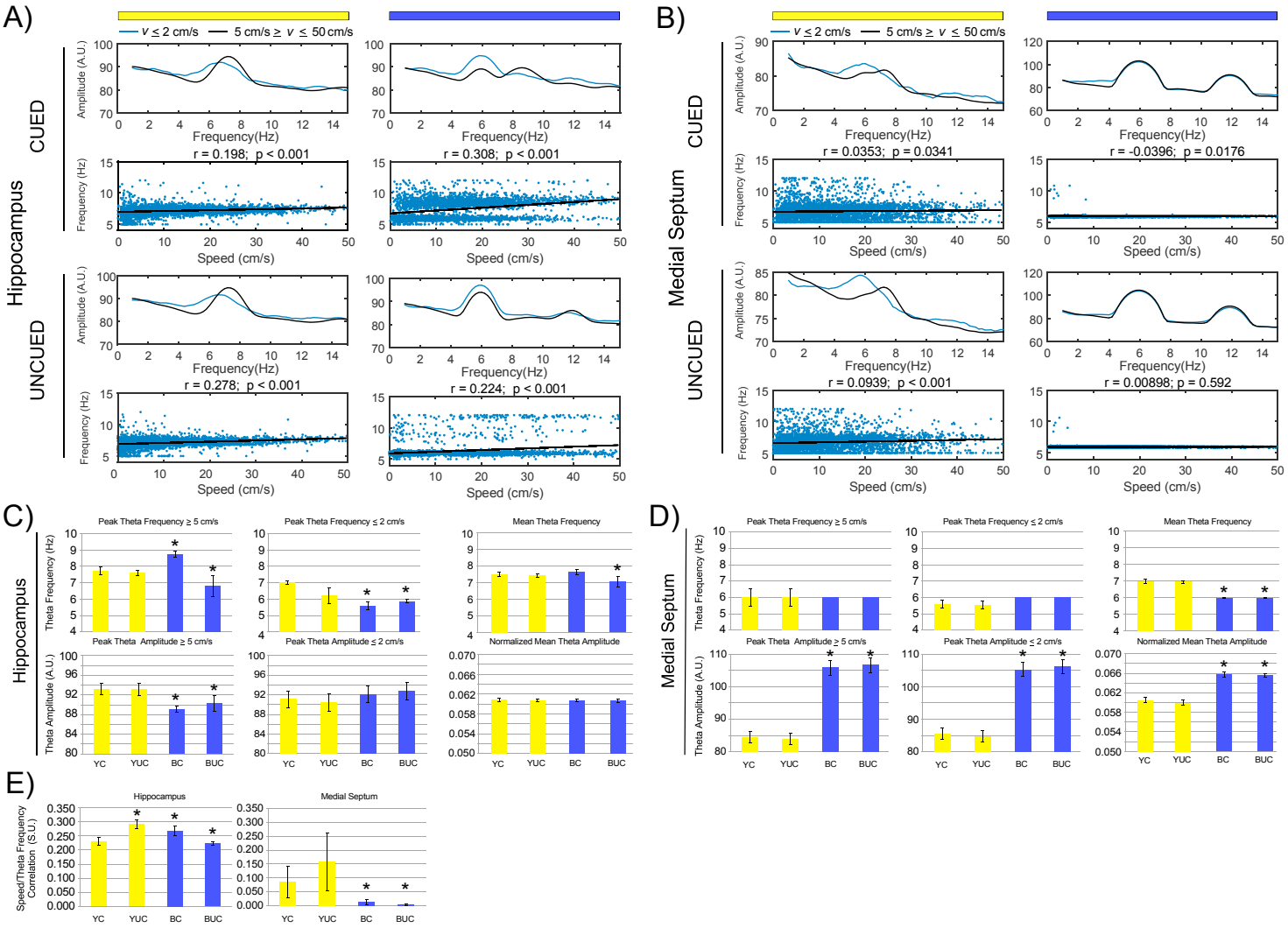
A)
v ≤ 2 cm/s
5 cm/s ≥ v ≤ 50 cm/s
Hippocampus
CUED
UNCUED
Amplitude (A.U.)
Frequency(Hz)
Frequency (Hz)
Speed (cm/s)
r = 0.198; p < 0.001
r = 0.308; p < 0.001
r = 0.278; p < 0.001
r = 0.224; p < 0.001
B)
Medial Septum
r = 0.0353; p = 0.0341
r = -0.0396; p = 0.0176
r = 0.0939; p < 0.001
r = 0.00898; p = 0.592
C)
Peak Theta Frequency ≥ 5 cm/s
Peak Theta Frequency ≤ 2 cm/s
Mean Theta Frequency
Peak Theta Amplitude ≥ 5 cm/s
Peak Theta Amplitude ≤ 2 cm/s
Normalized Mean Theta Amplitude
Theta Frequency (Hz)
Theta Amplitude (A.U.)
YC
YUC
BC
BUC
D)
E)
Hippocampus
Medial Septum
Speed/Theta Frequency Correlation (S.U.)

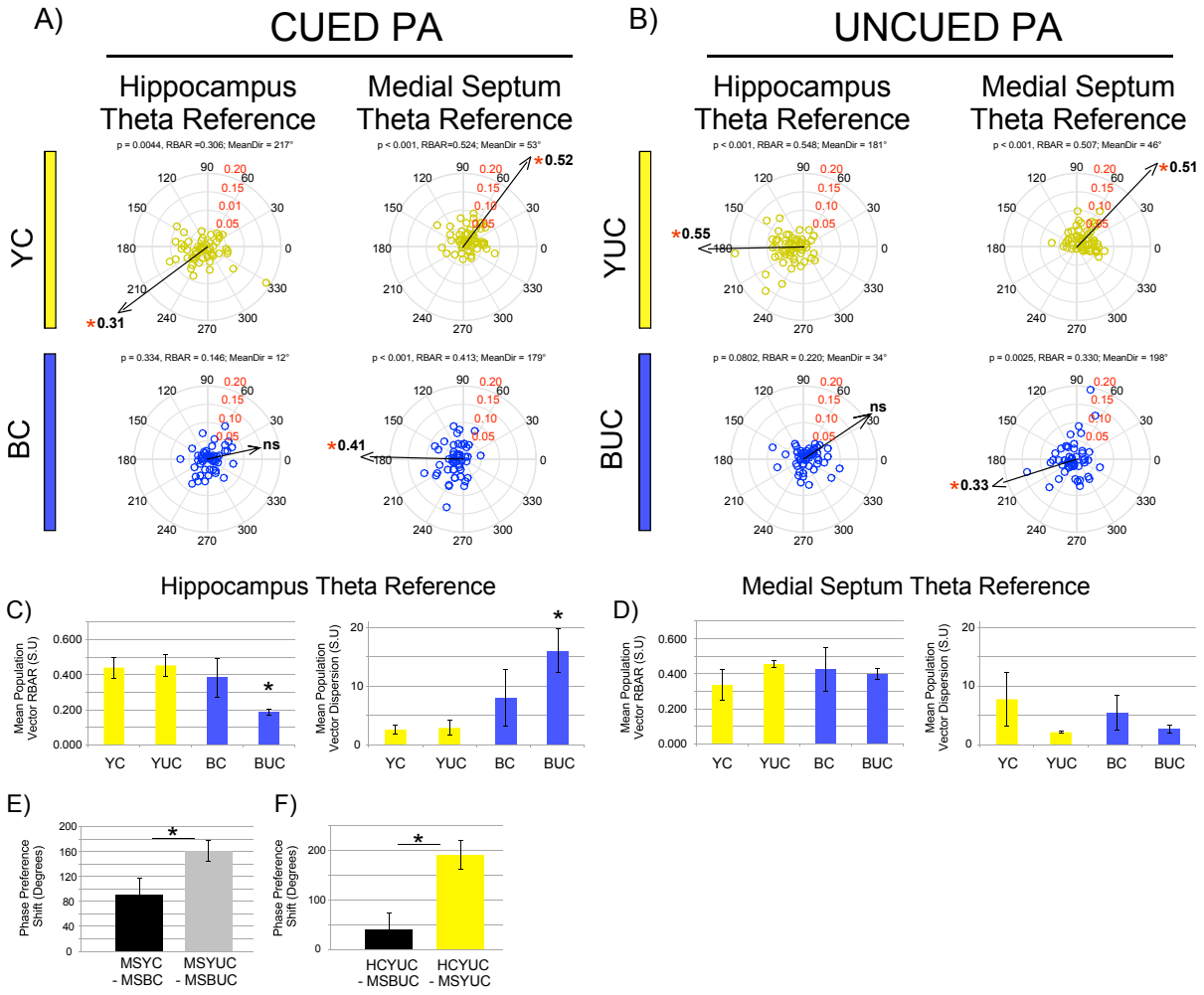
A)
CUED PA
Hippocampus Theta Reference
Medial Septum Theta Reference
B)
UNCUED PA
Hippocampus Theta Reference
Medial Septum Theta Reference
YC
BC
YUC
BUC
p = 0.0044, RBAR =0.306; MeanDir = 217°
*0.31
p < 0.001, RBAR=0.524; MeanDir = 53°
*0.52
p < 0.001, RBAR = 0.548; MeanDir = 181°
*0.55
p < 0.001, RBAR = 0.507; MeanDir = 46°
*0.51
p = 0.334, RBAR = 0.146; MeanDir = 12°
ns
p < 0.001, RBAR = 0.413; MeanDir = 179°
*0.41
p = 0.0802, RBAR = 0.220; MeanDir = 34°
ns
p = 0.0025, RBAR = 0.330; MeanDir = 198°
*0.33

Hippocampus Theta Reference
C)
Mean Population Vector RBAR (S.U)
Mean Population Vector Dispersion (S.U)
YC
YUC
BC
BUC
Medial Septum Theta Reference
D)
Mean Population Vector RBAR (S.U)
Mean Population Vector Dispersion (S.U)
YC
YUC
BC
BUC

E)
Phase Preference Shift (Degrees)
MSYC - MSBC
MSYUC - MSBUC
F)
Phase Preference Shift (Degrees)
HCYUC - MSBUC
HCYUC - MSYUC

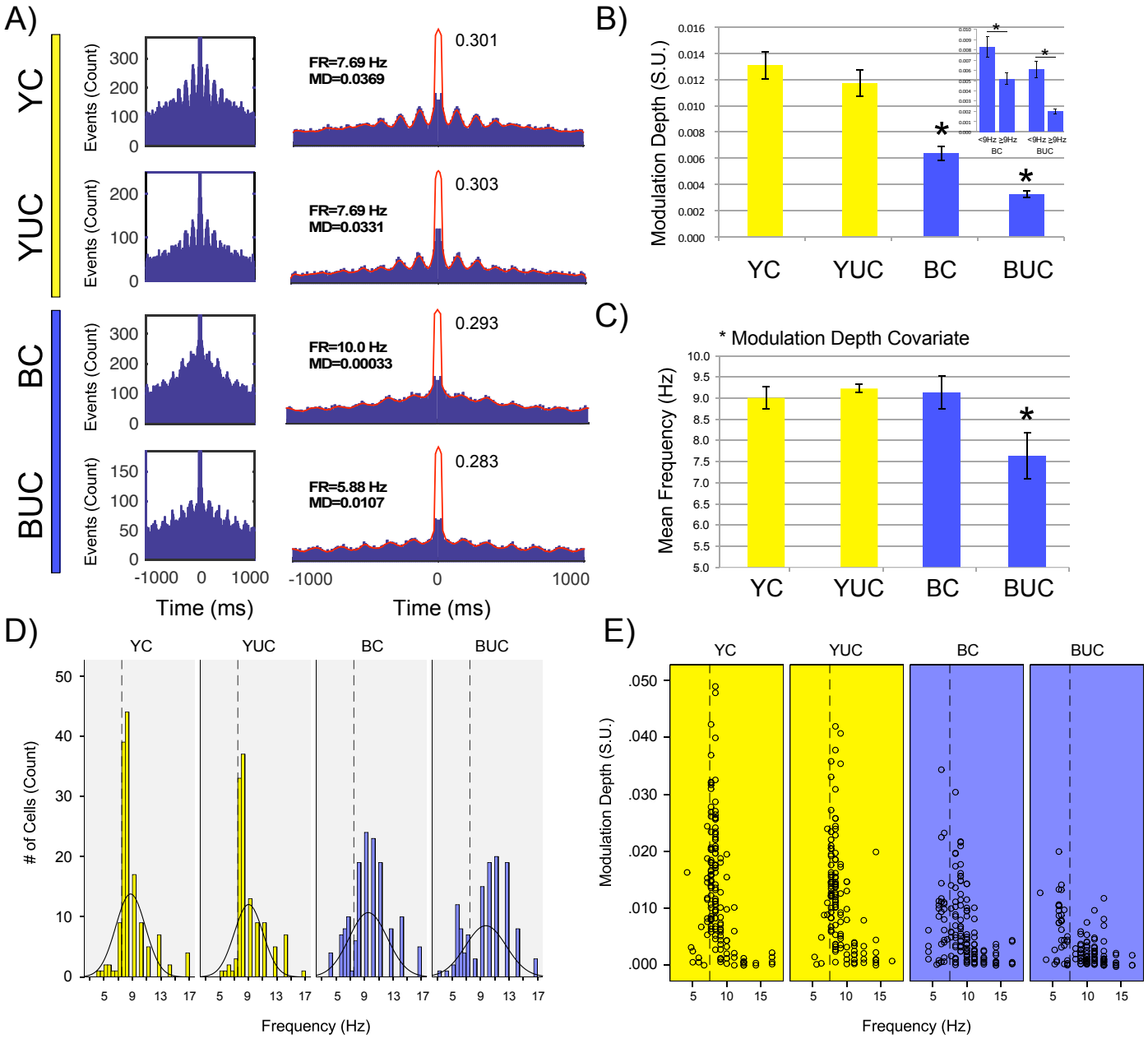
A)
YC
YUC
BC
BUC
Events (Count)
FR=7.69 Hz
MD=0.0369
0.301
FR=7.69 Hz
MD=0.0331
0.303
FR=10.0 Hz
MD=0.00033
0.293
FR=5.88 Hz
MD=0.0107
0.283
Time (ms)
B)
Modulation Depth (S.U.)
YC
YUC
BC
BUC
C)
* Modulation Depth Covariate
Mean Frequency (Hz)
D)
# of Cells (Count)
Frequency (Hz)
E)
Modulation Depth (S.U.)
Frequency (Hz)

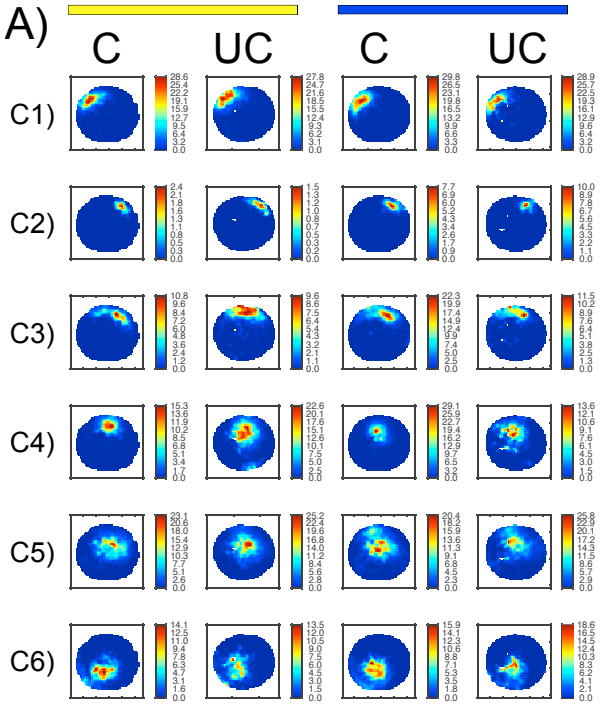
A)
C
UC
C
UC
C1)
C2)
C3)
C4)
C5)
C6)

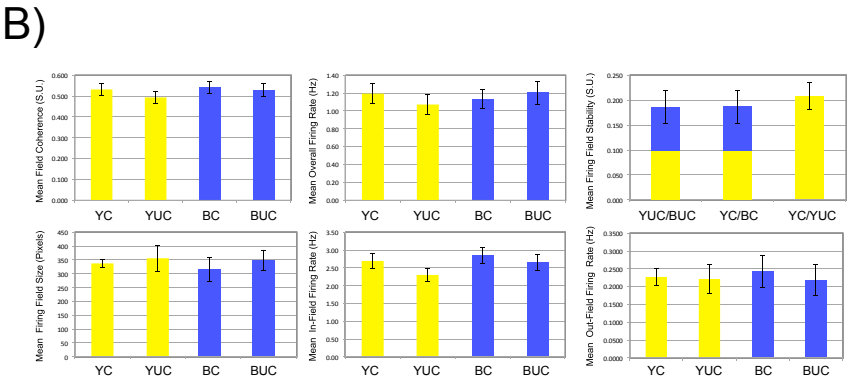
B)
Mean Field Coherence (S.U.)
Mean Overall Firing Rate (Hz)
Mean Firing Field Stability (S.U.)
Mean Firing Field Size (Pixels)
Mean In-Field Firing Rate (Hz)
Mean Out-Field Firing Rate (Hz)
YC
YUC
BC
BUC
YUC/BUC
YC/BC
YC/YUC

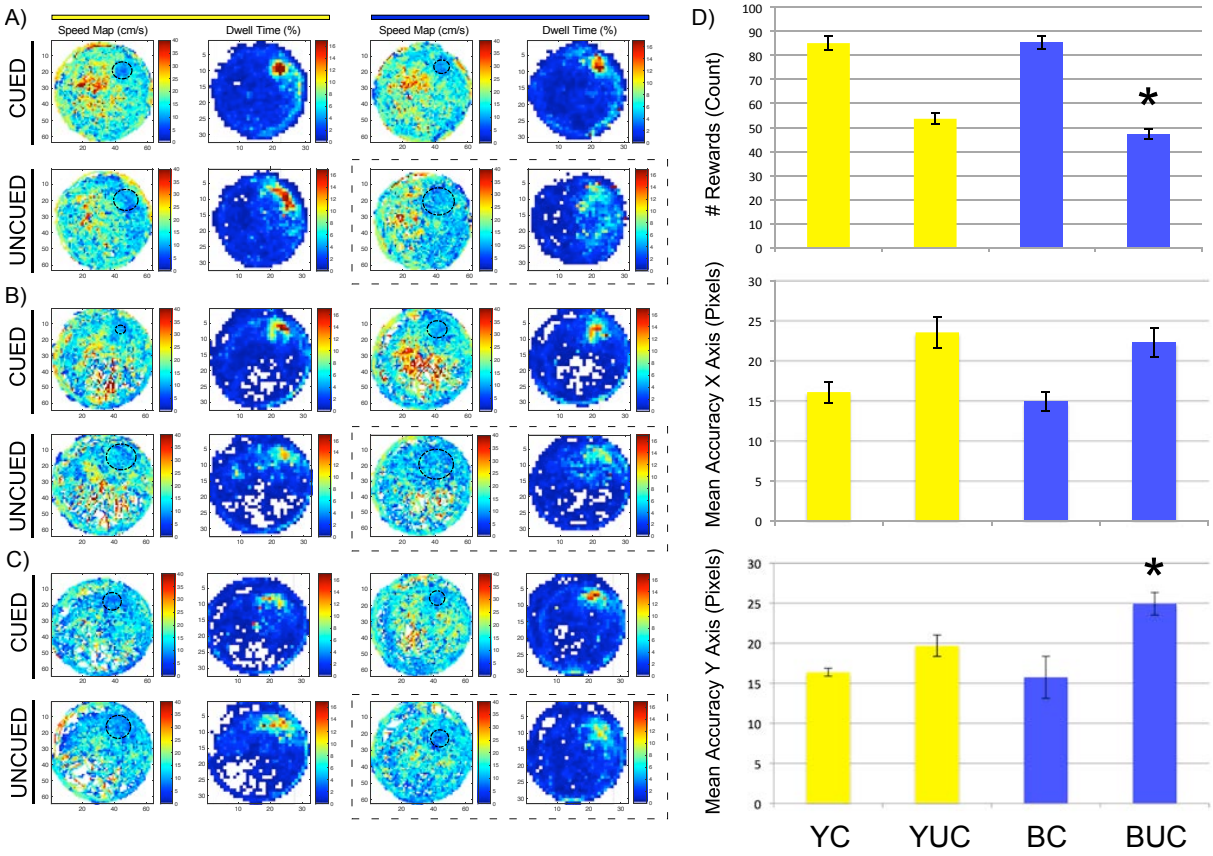
A)
Speed Map (cm/s)
Dwell Time (%)
Speed Map (cm/s)
Dwell Time (%)
CUED
UNCUED
B)
CUED
UNCUED
C)
CUED
UNCUED
D)
Rewards (Count)
Mean Accuracy X Axis (Pixels)
Mean Accuracy Y Axis (Pixels)
*
*
YC
YUC
BC
BUC

A)

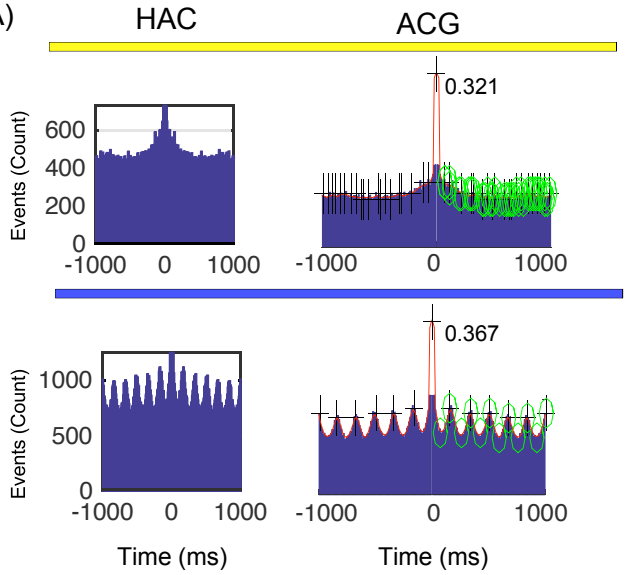

B)

	Y	B
Overall Rate (Hz)	0.3443	0.40678
Frequency (Hz)	12.5	6.25
Modulation Depth (S.U.)	0.0004994	0.045018

A)

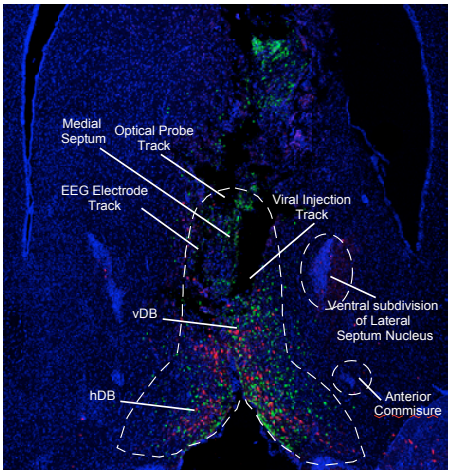
Medial Septum
Optical Probe Track
EEG Electrode Track
Viral Injection Track
vDB
Ventral subdivision of Lateral Septum Nucleus
hDB
Anterior Commisure

B)

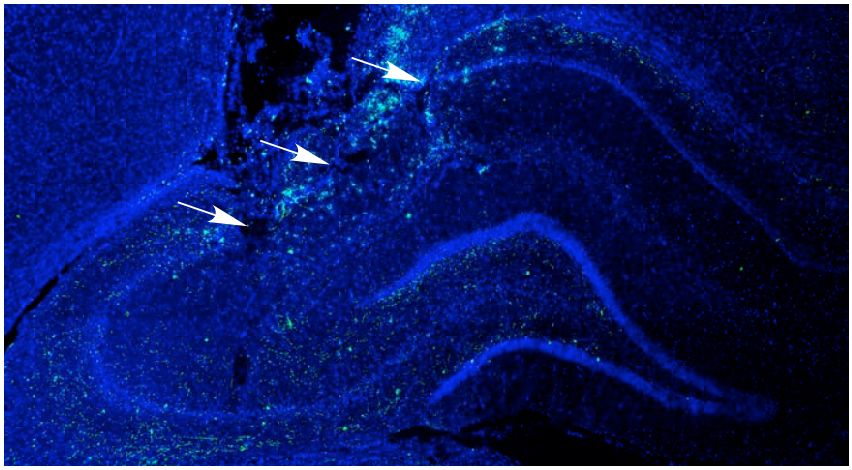

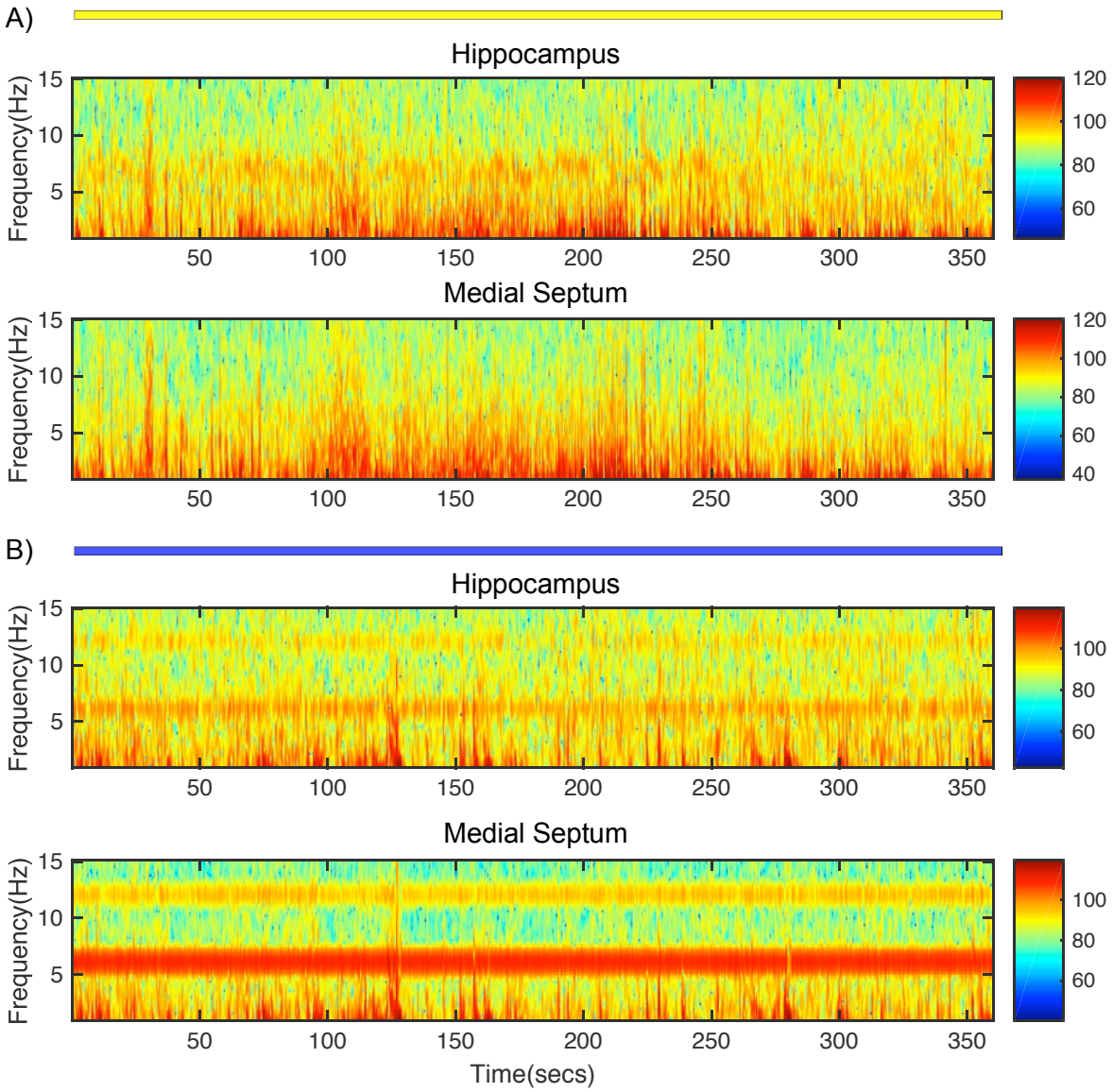
A)
Hippocampus
Frequency(Hz)
15
10
5
50
100
150
200
250
300
350
120
100
80
60
Medial Septum
Frequency(Hz)
15
10
5
50
100
150
200
250
300
350
120
100
80
60
40
B)
Hippocampus
Frequency(Hz)
15
10
5
50
100
150
200
250
300
350
100
80
60
Medial Septum
Frequency(Hz)
15
10
5
50
100
150
200
250
300
350
Time(secs)
100
80
60

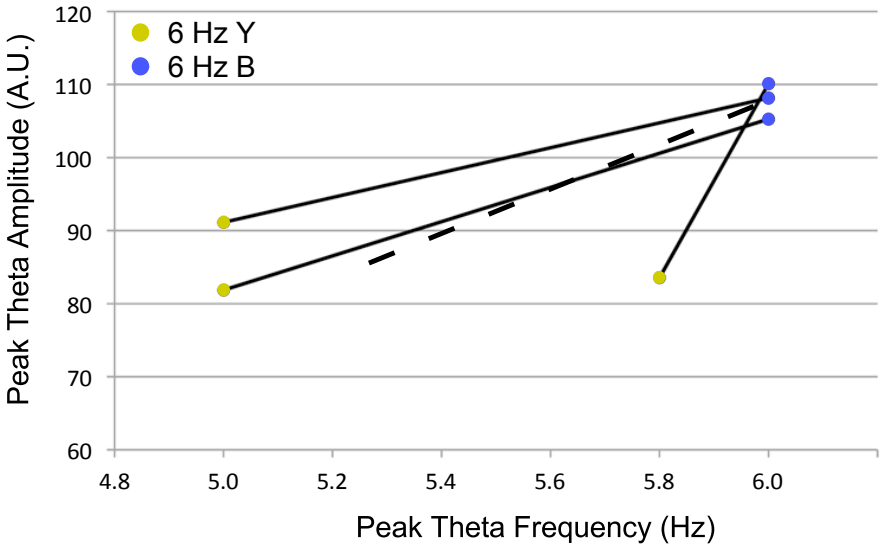
6 Hz Y
6 Hz B
Peak Theta Amplitude (A.U.)
120
110
100
90
80
70
60
4.8
5.0
5.2
5.4
5.6
5.8
6.0
Peak Theta Frequency (Hz)

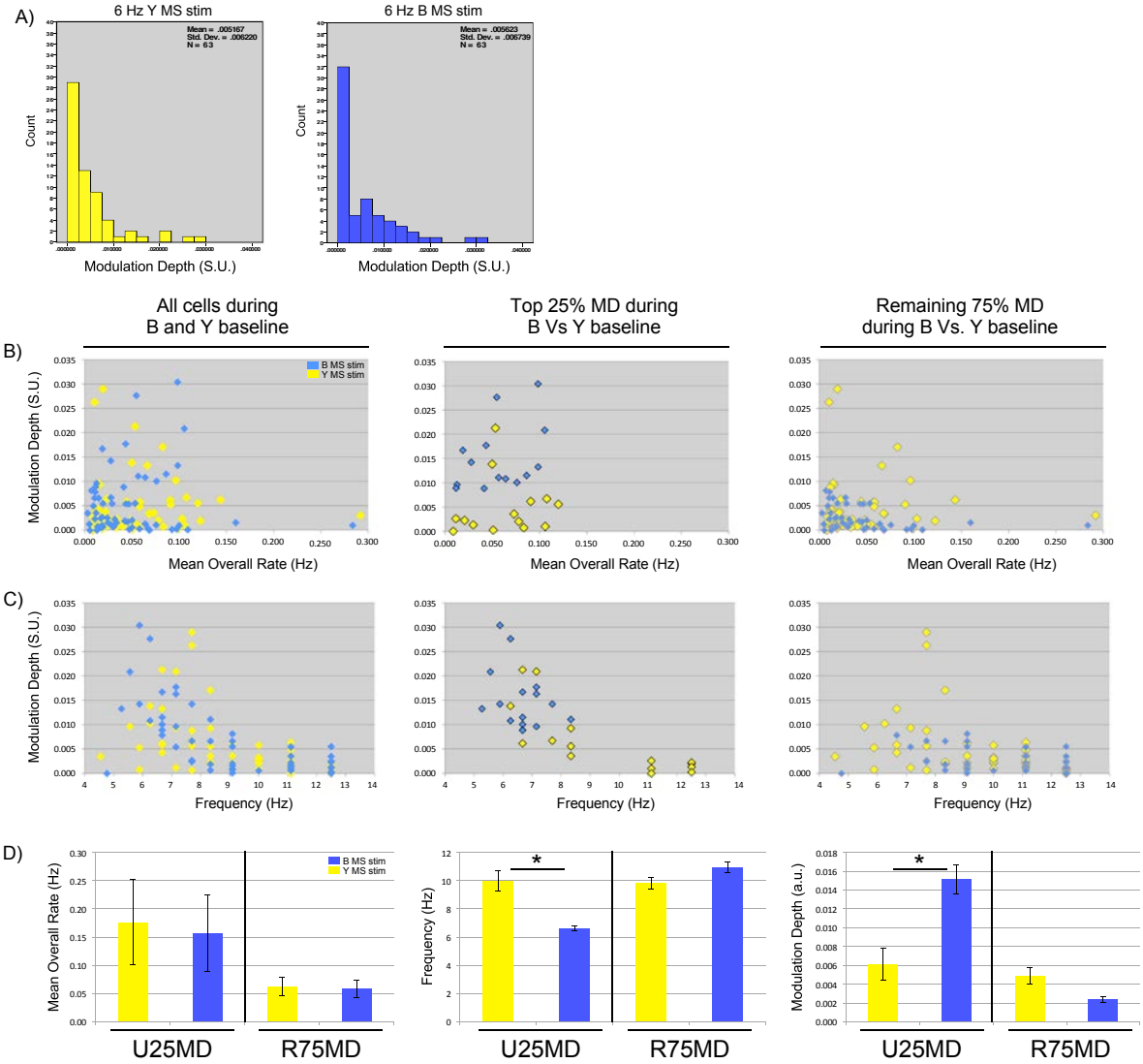
A)
6 Hz Y MS stim
Mean = .005167
Std. Dev. = .006220
N = 63
Count
Modulation Depth (S.U.)
6 Hz B MS stim
Mean = .005623
Std. Dev. = .006739
N = 63
Count
Modulation Depth (S.U.)
B)
All cells during B and Y baseline
Top 25% MD during B Vs Y baseline
Remaining 75% MD during B Vs. Y baseline
B MS stim
Y MS stim
Modulation Depth (S.U.)
Mean Overall Rate (Hz)
C)
Modulation Depth (S.U.)
Frequency (Hz)
D)
B MS stim
Y MS stim
Mean Overall Rate (Hz)
Frequency (Hz)
Modulation Depth (a.u.)
*
*
U25MD
R75MD
U25MD
R75MD
U25MD
R75MD

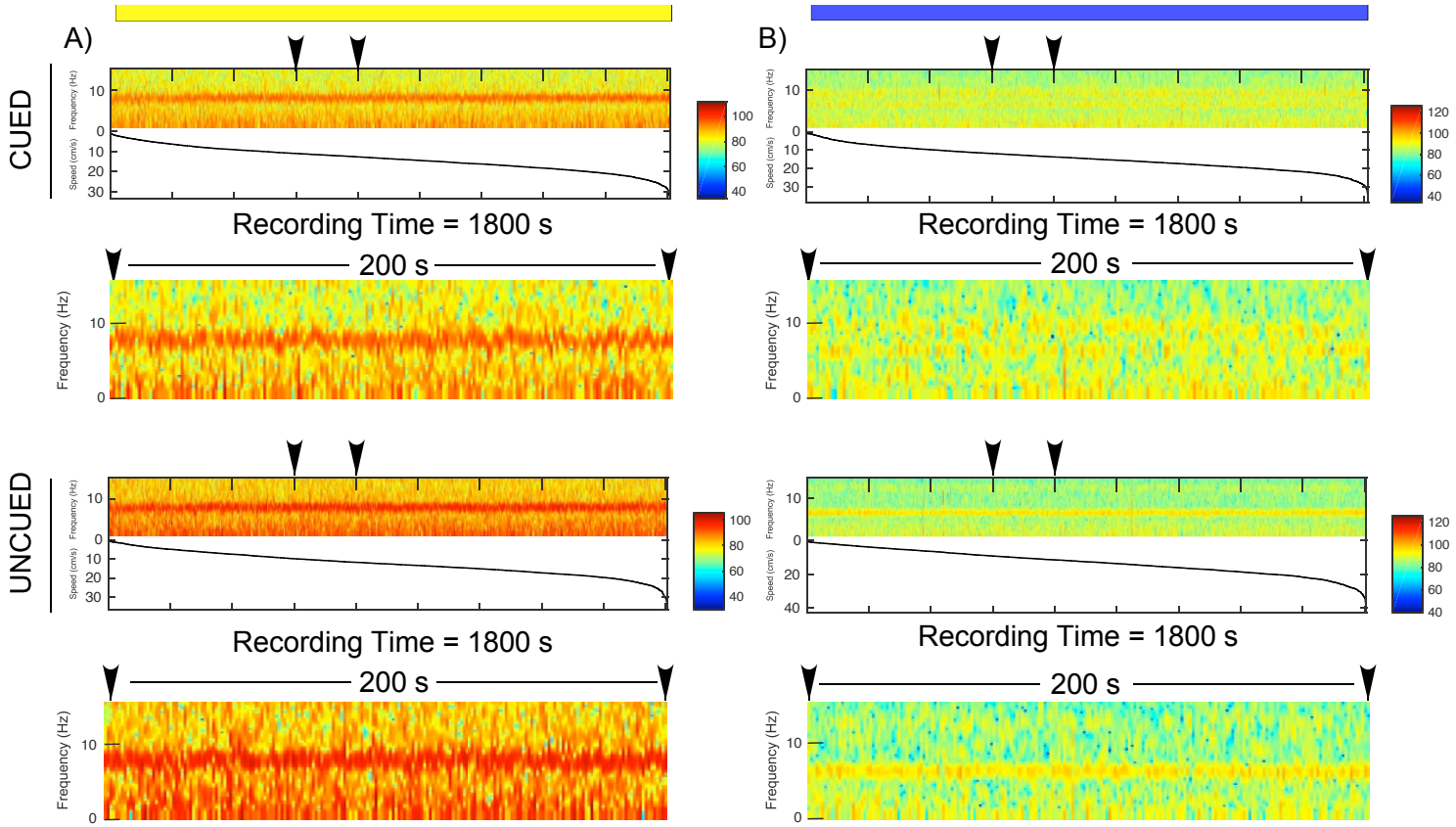
A)
B)
CUED
UNCUED
Frequency (Hz)
Speed (cm/s)
Recording Time = 1800 s
200 s
Frequency (Hz)

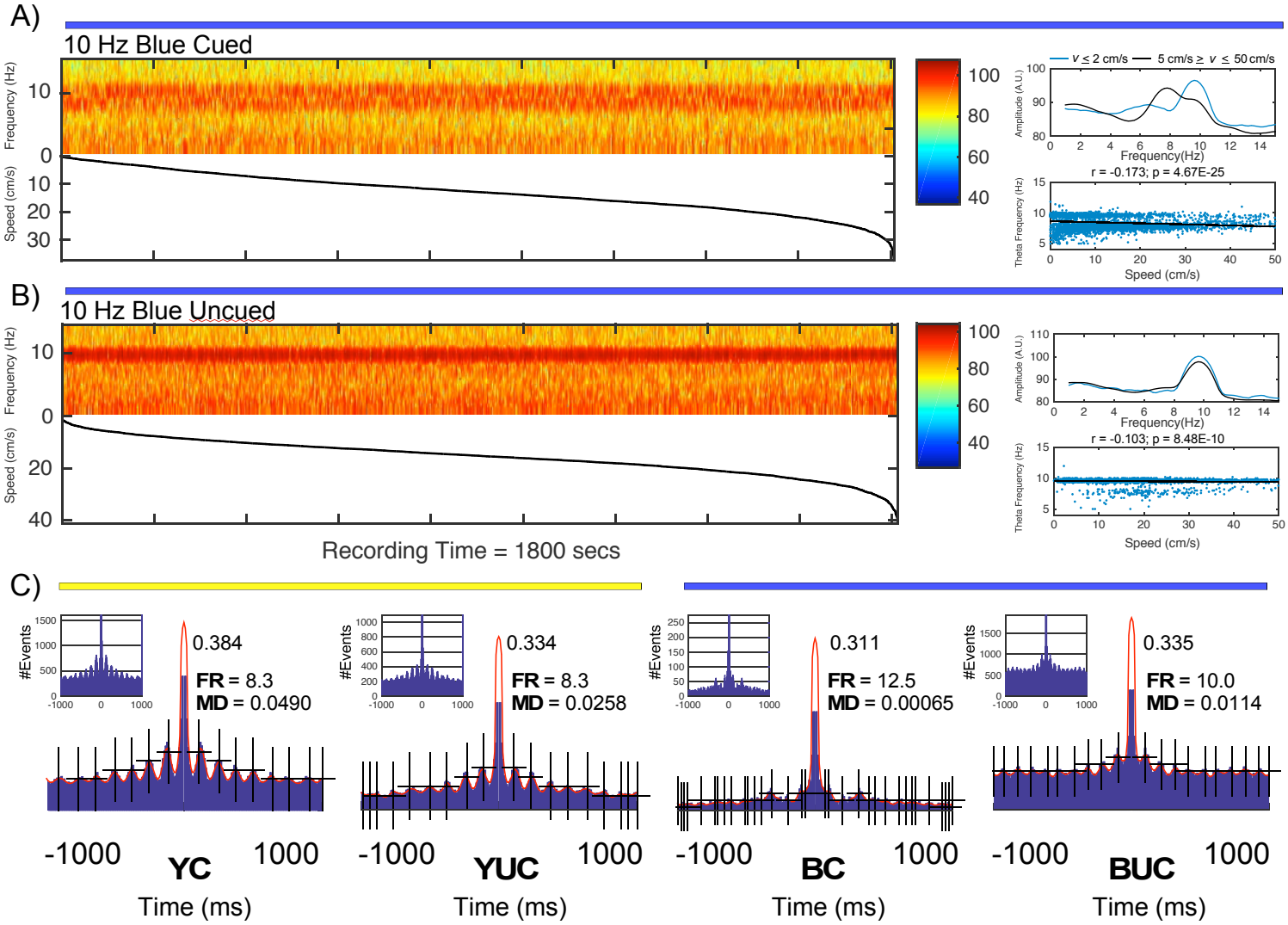

Table 1

	Speed (cm/s)	Speed/Theta r (S.U.)	
BC	12.88 ± 1.72	-0.035 ± 0.057	
BUC	13.92 ± 1.85	-0.042 ± 0.034	
	Peak Theta F (Fast)	Peak Theta F (Slow)	Mean Theta F
BC	9.00 ± 0.499 Hz	8.07 ± 1.25 Hz	8.41 ± 0.267 Hz
BUC	9.60 ± 0.0 Hz	9.6 ± 0.0 Hz	8.81 ± 0.419 Hz
	Peak Theta Amp. (Fast)	Peak Theta Amp. (Slow)	Normalized Mean Theta Amp.
BC	90.75 ± 2.30	92.28 ± 3.65	0.0600 ± 0.00100
BUC	91.95 ± 2.98	93.81 ± 3.71	0.0599 ± 0.00087

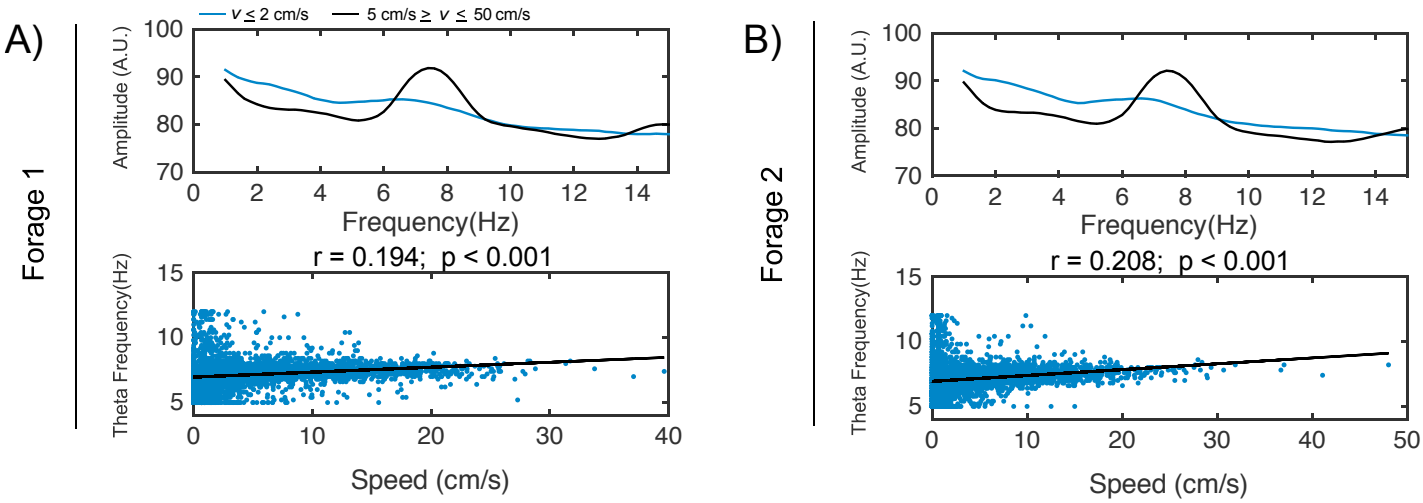

Table 2

	Speed (cm/s)	Speed/Theta r (S.U.)	
Forage 1	9.97 ± 2.87	0.225 ± 0.045	
Forage 2	9.18 ± 2.87	0.215 ± 0.043	
	Peak Theta F (Fast)	Peak Theta F (Slow)	Mean Theta F (Fast)
Forage 1	7.60 ± 0.143 Hz	6.60 ± 0.230 Hz	7.56 ± 0.103 Hz
Forage 2	7.73 ± 0.150 Hz	6.93 ± 0.241 Hz	7.59 ± 0.103 Hz
	Peak Theta Amp. (Fast)	Peak Theta Amp. (Slow)	Normalized Mean Theta Amp. (Fast)
Forage 1	95.55 ± 1.97	91.33 ± 3.09	0.0608 ± 0.000773
Forage 2	95.48 ± 1.97	91.94 ± 3.11	0.0608 ± 0.000773

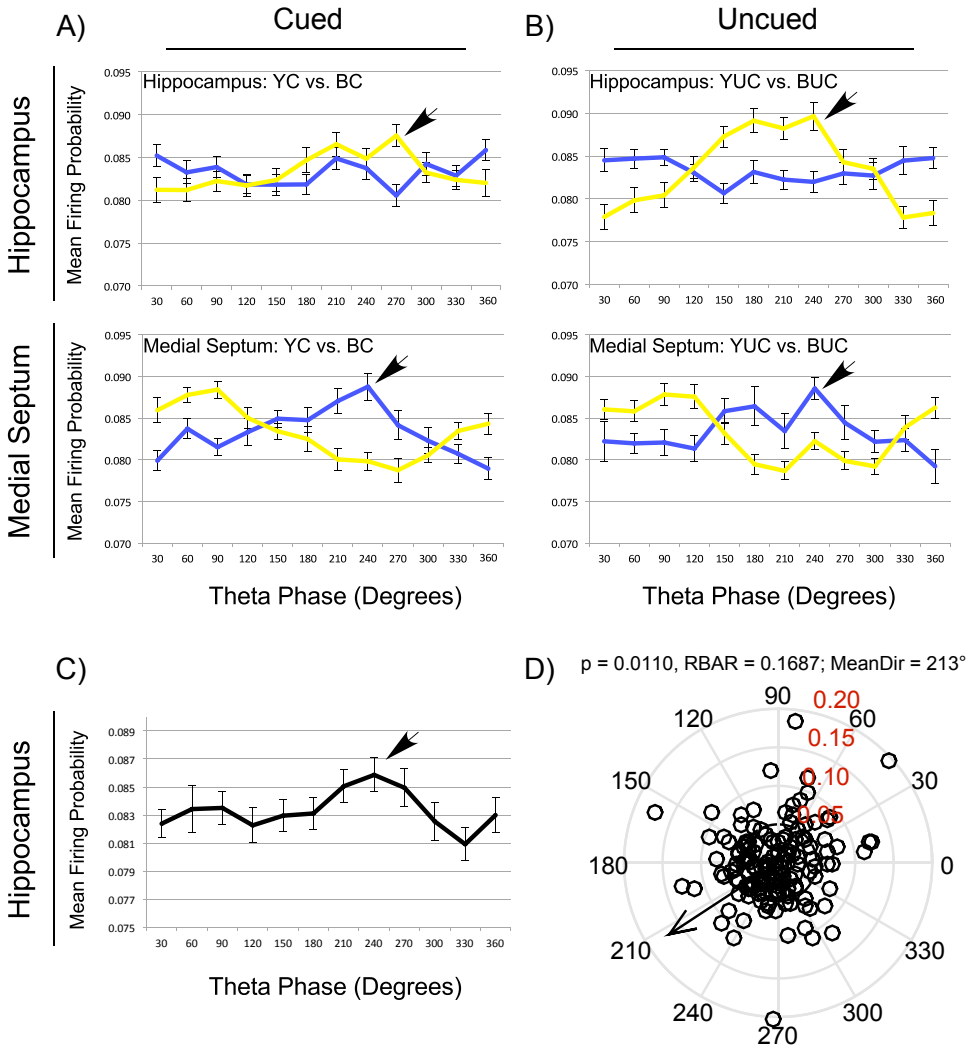
A)
Cued
B)
Uncued
Hippocampus
Medial Septum
Mean Firing Probability
Hippocampus: YC vs. BC
Hippocampus: YUC vs. BUC
Medial Septum: YC vs. BC
Medial Septum: YUC vs. BUC
Theta Phase (Degrees)
Theta Phase (Degrees)
C)
D)
p = 0.0110, RBAR = 0.1687; MeanDir = 213°

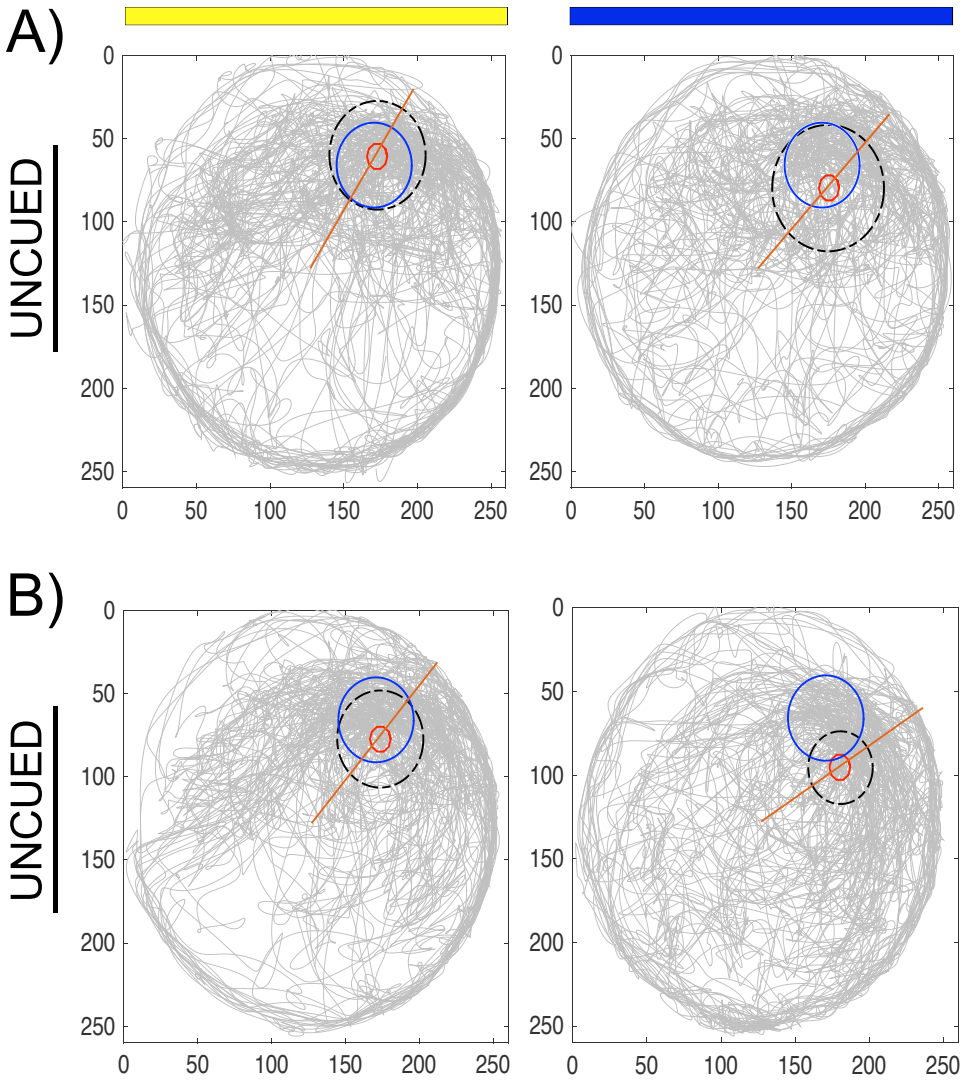
A)
UNCUED
B)
UNCUED
0
50
100
150
200
250